«ФИЗИКА ЭЛЕМЕНТАРНЫХ ЧАСТИЦ И АТОМНОГО ЯДРА»
1997, ТОМ 28, ВЫП.6

УДК 539.142 +
539.143.43

MAGNETIC DIPOLE EXCITATIONS IN DEFORMED NUCLEI

N. Lo Iudice

Dipartimento di Scienze Fisiche, Universitá di Napoli «Federico II»
and Istituto Nazionale di Fisica Nucleare, Mostra d'Oltremare Pad. 19, I-80125 Napoli, Italy

The many models adopted to study the properties of the low-lying magnetic dipole excitations known as scissors mode observed in most deformed nuclei are reviewed. Attention is focused first on the geometrical two-rotor model (TRM) whose predictions gave the motivation for searching for such a mode. The consistency of these predictions with the most meaningful collective properties of the mode is emphasized. More sophisticated descriptions carried out within different Boson models are then reviewed. Their strict connection with the TRM is proved. An even closer link is shown to exist between the TRM and schematic random-phase approximation (RPA). From the phenomenological and schematic models, confined to the description of the collective features of the $M1$ transitions, the analysis moves to the fully microscopic approaches, the only ones capable of accounting for the global properties of the mode as well as for the fragmentation of its $M1$ strength. shell-model approaches, widely adopted for light and medium-light nuclei, are discussed. A more detailed analysis is devoted to the RPA, the most widely adopted microscopic scheme, especially in heavy nuclei. The path leading from the early incomplete and too approximate approaches yielding contradictory results to the most recent and refined studies converging to similar conclusions is sketched. The quasiparticle-phonon model (QPNM) as a way of improving the RPA description of the $M1$ spectrum by including the coupling with two-phonon RPA states, is finally illustrated and the related results are discussed. The study of the $M1$ spectra observed recently in deformed odd-mass nuclei carried out in a QPNM context completes the review.

Рассмотрены свойства низколежащих магнитных дипольных возбуждений, обнаруженных недавно во многих деформированных ядрах экспериментально и названных «ножничной» модой. Представлен обзор ряда моделей, применяемых для изучения указанных состояний. Прежде всего дано описание двухроторной модели (ДРМ), предсказания которой послужили основанием для поиска этой новой коллективной ядерной моды. Проанализированы другие феноменологические и микроскопические ядерные модели, и показана их связь с ДРМ. Детально рассмотрено приближение случайных фаз (ПСФ), наиболее разработанное направление в теории, особенно для тяжелых ядер. Продемонстрированы пути улучшения ПСФ, выполненные в квазичастично-фононной модели ядра (КФМЯ) посредством учета связи с двухфононными конфигурациями. Проведено сравнение $M1$-спектров, измеренных недавно в деформированных A-нечетных ядрах, с рассчитанными в КФМЯ.

1. INTRODUCTION

The field of magnetic dipole response has expanded considerably its scope since the discovery of low-lying $M1$ excitations, known as scissors mode, made by Richter and coworkers in ^{156}Gd through a high-resolution inelastic electron scattering experiment [1]. The search for such a mode was stimulated by the prediction, made within the TRM [2], of a collective $M1$ mode promoted by a rotational oscillation of proton versus neutron deformed fluids. The name «scissors mode» was indeed suggested by such a geometrical picture. A magnetic excitation of similar nature was predicted as mixed-symmetry state in the proton-neutron interacting boson model (IBM2) [3,4] and as giant angle resonance in a schematic model [5].

The discovery has led to a renaissance of low-energy nuclear spectroscopy. Not only electron scattering but also nuclear resonance fluorescence (NRF) and proton scattering have been adopted for a systematic search of this new mode. As summarized in several review articles [6—10], the mode has been detected in most of the deformed nuclei ranging from the fp-shell to rare-earth and actinide regions. The search has also stimulated important advances in the experimental techniques which have enabled a quite complete characterization of the mode. It is well established by now that this is fragmented into several closely packed $M1$ transitions. These are mainly promoted by the convection current, and their summed $M1$ strength grows quadratically with the nuclear deformation parameter. This latter property was found recently in the rare-earth region [11—15] and represents the most spectacular signature of the mode.

With the use of Compton polarimeters in NRF which has enabled parity assignment [16], unexpectedly strong $E1$ transitions in the same energy range of the scissors mode, or immediately below, have been detected [17—20].

Another byproduct of the systematic study of the mode has been the discovery of spin excitations. Inelastic proton scattering experiments on ^{154}Sm and other deformed nuclei [21], have found a sizeable, strongly fragmented, $M1$ spin strength distributed over an energy range of 4 to 12 MeV so as to give rise to a double-hump [22].

The experimental discovery has stimulated a proliferation of theoretical investigations. The gross features of the mode were analysed in several phenomenological models. We recall, among them the IBM2 [23—29], the extended Bohr–Mottelson model [30], the closely related neutron-proton deformation model (NPD) [31], and the generalized coherent state model (CGSM) [32,33]. Studies carried out in a sum rule approach [34], in schematic random-phase approximation [35—37] and in a mean field context [38] have given illuminating insights on the shell structure of the mode.

Phenomenological and schematic models ignore many degrees of freedom, such as spin. For this reason they are inadequate for describing the detailed structure of the mode. An exhaustive analysis covering also the energy strength distribution can be carried out only in fully microscopic approaches.

Microscopic calculations were performed in the context of standard shell-model for medium-light nuclei [39—42]. These can be viewed as the microscopic counterpart of an extended version of the interacting boson model, the IBM3, also used to study the $M1$ mode in the same nuclei [43,44]. An alternative and valid approach for this nuclear region has consisted in adopting an $SU(3)$ shell model basis [45—47]. The same $SU(3)$ scheme was modified so as to enable the description of the mode also in heavy nuclei [48,49]. In heavy deformed nuclei, however, apart from few exceptions [50,51], most of the microscopic studies were carried out in RPA [52—77] or in Tamm-Dancoff approximation (TDA) [78,79].

A new boost to theoretical studies has been stimulated by the discovery of the quadratic deformation law. This property has been studied in practically all models adopted previously either in the microscopic [42,69,74,77,79—83] or phenomenological domain [79,84—92]. All these analyses give a conclusive support to the scissors nature of the magnetic transitions found experimentally. Nonetheless, a complete detailed understanding of the related phenomenology is still lacking. The present situation is in fact more complex than that of the $E1$ resonance. Unlike in the case of the $E1$ mode, the $M1$ transitions lead to bound states, so that the theoretical models have to reproduce the pattern of fragmentation instead of a broad peak. Another feature of the $M1$ mode which complicates its description is, for example, the interplay between spin and orbital motion. Because of the many degrees of freedom involved in the transitions, several components of the nuclear Hamiltonian enter into play in determining the size and the distribution pattern of the strength. All these aspects are taken into account in RPA calculations. These, however, being confined within a space spanned by two quasiparticle states, may miss some configurations which enter into the $M1$ channel either directly or through coupling.

An effort for improving and extending the TDA and RPA calculations has been made recently by studying the mode within the quasiparticle-phonon nuclear model (QPNM) [93] which accounts for the coupling with two RPA phonons [94].

Theoretical studies have also posed the question of whether the scissors mode survives as one moves from even- to odd-mass nuclei [95—98]. After a first negative attempt carried out in electron scattering [99], NRF experiments have detected in several odd-mass deformed nuclei of the rare-earth region a sizeable dipole strength whose distribution pattern follows closely the $M1$ spectrum of the nearby even mass partners [20,100,101]. Schematic and phenomenological models are even more inadequate for facing the extreme complexity

of the $M1$ spectrum in odd-mass nuclei. Fully microscopic calculations are badly needed for this purpose. The first and only calculation of this kind has been carried out recently using the QPNM formalism [102,103].

Section 2 deals with the TRM prediction and the experimental evidence of the mode. The systematic experimental analyses are briefly reviewed. The consistency of the model with the deformation law is discussed. Its microscopic formulation is illustrated. In Sec. 3 the description of the mode within different Boson models is discussed. The analysis covers the extended Bohr–Mottelson, the NPD, the GCSM and the algebraic IBM2 models. The review then moves to shell-model studies (Sec. 4). Standard as well as $SU(3)$ shell model calculations are presented. The microscopic investigations go on with RPA. The method, the problem, the early calculations have run into, the way of solving them and, finally, the most meaningful results are discussed in Section 5. We go then beyond RPA by reviewing briefly the QPNM and by discussing the results obtained in relation to experiments and RPA (Sec. 6). The review is completed by the discussion of the $M1$ spectra observed in deformed odd-mass nuclei and studied within the QPNM formalism in Sec. 7. Conclusions are drawn in the final Section 8.

2. SCISSORS MODE: PREDICTION AND EXPERIMENTAL EVIDENCE

The angular momentum carried out by the nucleus does not produce any intrinsic excitation. This reflects the spherical symmetry of the nuclear Hamiltonian just as its translational invariance forbids the occurrence of an isoscalar collective $E1$ mode. One may however carry further the analogy with translations and assume that protons and neutrons form two distinct deformed fluids free to rotate separately about a common axis (perpendicular to their symmetry axes). Because of their mutual interaction, they may undergo a rotational oscillation giving rise to an intrinsic $M1$ excitation. This is the underlying idea of the TRM [2] which represents the rotational counterpart of the semiclassical picture of the $E1$ giant resonance [104,105].

A. TRM Prediction of the Scissors Mode. The Hamiltonian describing two axially symmetric rotors interacting via a potential $V(\vartheta)$ dependent on the angle 2ϑ between the symmetry axes has the form

$$H_{TR} = \frac{1}{2\Im_p}\mathbf{J}_p^2 + \frac{1}{2\Im_n}\mathbf{J}_n^2 + V(\vartheta), \tag{2.1}$$

where $\Im_p$ and $\Im_n$ are the proton and neutron moments of inertia, $\mathbf{J}_p$ and $\mathbf{J}_n$ are their angular momenta.

Expressed in terms of the total and relative angular momenta

$$\mathbf{J} = \mathbf{J}_p + \mathbf{J}_n\,, \quad \mathbf{S} = \mathbf{J}_p - \mathbf{J}_n \tag{2.2}$$

the Hamiltonian decouples into a rotational and an intrinsic part, if a Coriolis-like term is neglected. For small values of ϑ, the intrinsic piece assumes the form of a two-dimensional harmonic oscillator (HO) Hamiltonian

$$H = H_{\text{int}} = \frac{1}{2\Im_{\text{sc}}}(S_1^2 + S_2^2) + \frac{1}{2} C_\vartheta(\vartheta_1^2 + \vartheta_2^2), \tag{2.3}$$

where ϑ_k ($k = 1, 2$) play the role of x and y variables and

$$S_k = J_k^{(p)} - J_k^{(n)} = i\frac{d}{d\vartheta_k} \tag{2.4}$$

are their conjugate momenta. The TRM physical constants are

$$\Im_{\text{sc}} = \frac{4\Im_p \Im_n}{\Im_p + \Im_n}\,, \quad C_\vartheta = \Im_{\text{sc}}\omega^2 = \frac{4C_\vartheta^{(p)} C_\vartheta^{(n)}}{C_\vartheta^{(p)} + C_\vartheta^{(n)}}\,, \tag{2.5}$$

where we have put $C_\vartheta^{(\tau)} = \omega^2 \Im_\tau$ with $\tau = p$ for protons and $\tau = n$ for neutrons.

The energy eigenvalues are

$$\omega_{nK} = \omega(2n + K + 1). \tag{2.6}$$

The scissors mode corresponds to the first excited level. Its quantum numbers $n = 0$ and $K = 1$ define a positive parity band of intrinsic excitation energy ω. In order to illustrate the mechanism of excitation we decompose the TRM $M1$ operator as follow

$$\mathcal{M}(M1, \mu) = \sqrt{\frac{3}{4\pi}}\,(g_p J_\mu^{(p)} + g_n J_\mu^{(n)})\,\mu_N =$$

$$= \mathcal{M}_J(M1, \mu) + \mathcal{M}_{\text{sc}}(M1, \mu). \tag{2.7}$$

The first piece is the rotational component

$$\mathcal{M}_J(M1, \mu) = \sqrt{\frac{3}{4\pi}}\,J_\mu\, g_R\, \mu_N\,, \tag{2.8}$$

where $g_R = (g_p + g_n)/2$ is the rotational gyromagnetic factor. The second is the scissors $M1$ component

$$\mathcal{M}_{sc}(M1, \mu) = \sqrt{\frac{3}{16\pi}}\, S_\mu\, g_r\, \mu_N, \tag{2.9}$$

where $g_r = g_p - g_n$. This term is responsible for the excitation of the mode. In order to compute the transition strength one may exploit the harmonic relations holding for the TRM Hamiltonian

$$\frac{1}{\mathfrak{I}_{sc}} \langle S^2 \rangle = \frac{1}{\mathfrak{I}_{sc}} \sum_{\mu=\pm 1} |\langle \mu | S_\mu | 0 \rangle|^2 = \omega,$$

$$C = \omega \sum_{\mu=\pm 1} |\langle \mu | S_\mu | 0 \rangle|^2. \tag{2.10}$$

In view of the structure of the scissors $M1$ operator (2.9), the above equations yield for the $M1$ strength the expression

$$B(M1)\uparrow = \frac{3}{16\pi} \sum_{\mu=\pm 1} |\langle \mu | S_\mu | 0 \rangle|^2 g_r^2\, \mu_N^2 = \frac{3}{16\pi}\, \mathfrak{I}_{sc}\, \omega g_r^2\, \mu_N^2. \tag{2.11}$$

The mode can be further characterized by the $M1$ form factor. The general expression of the magnetic orbital operator for electron scattering is

$$T_\mu^{(\lambda)}(q) = -\frac{i}{\sqrt{\lambda(\lambda+1)}} \int d\mathbf{r} \mathbf{j}_p(\mathbf{r}) \cdot \mathbf{r} \times \nabla (j_\lambda(qr)\, Y_{\lambda\mu}) =$$

$$= -\frac{i}{\sqrt{\lambda(\lambda+1)}} \int d\mathbf{r} \rho_p(\mathbf{r})\, \mathbf{v}_p(\mathbf{r}) \cdot (\mathbf{r} \times \nabla)(j_\lambda(qr)\, Y_{\lambda\mu}) =$$

$$= -\frac{1}{m} \frac{i}{\sqrt{\lambda(\lambda+1)}} \int d\mathbf{r} \rho_p(\mathbf{r})\, \mathbf{l}_p \cdot \nabla (j_\lambda(qr)\, Y_{\lambda\mu}), \tag{2.12}$$

where m and $\mathbf{l}_p$ are the proton mass and angular momentum, respectively.

The transition operator can be conveniently rewritten by using the classical relations

$$\mathbf{l} = m\mathbf{r}(\mathbf{r} \cdot \boldsymbol{\Omega}) - mr^2 \boldsymbol{\Omega},$$

$$\boldsymbol{\Omega}_p = \frac{1}{\mathfrak{I}_p} \mathbf{I}_p. \tag{2.13}$$

After some straightforward algebra we obtain ($\mu = \pm 1$)

$$T_\mu^{(\lambda)}(q) = \frac{i}{\sqrt{2\lambda(\lambda+1)}} S_\mu \frac{1}{\mathfrak{I}_p} \int d\mathbf{r} \rho_p(\mathbf{r}) \frac{j_\lambda(qr)}{r^\lambda} (r^2 \partial_1 - x_1 \mathbf{r} \cdot \nabla)(r^\lambda Y_{\lambda\mu}). \tag{2.14}$$

For $\lambda = 1$ the only nonvanishing matrix element is

$$\langle I = K = 1, n = 0 \| \; T^{(\lambda)}(q) \| \; I = K = n = 0 \rangle =$$

$$= -\sqrt{\frac{\pi}{3}} \sqrt{\frac{\omega}{\Im}} \int_0^\infty dr r^3 \rho(r) j_1(qr), \tag{2.15}$$

where $\rho(r)$ is a spherical density normalized to the total number of nucleons.

For $\lambda > 1$ the integral in eq. (2.14) vanishes unless the density deformation is taken into account. To this purpose [106] let us consider a proton (neutron) density of the form suitable to an axially deformed shape

$$\rho_\tau(\mathbf{r}) = \rho_\tau[r - R(1 + \alpha_{20}^{(\tau)} Y_{20}(\hat{r}))], \tag{2.16}$$

where

$$\alpha_{20}^{(\tau)} = \beta_\tau = \sqrt{\frac{16\pi}{45}} \, \delta_\tau . \tag{2.17}$$

For $\lambda = 3$ the only nonvanishing matrix element is [106]

$$\langle I = 3 K = 1 n = 0 \| \; T^{(\lambda=3)}(q) \| \; I = K = n = 0 \rangle =$$

$$= \frac{4}{15} \sqrt{\frac{2\pi}{7}} \, \delta \sqrt{\frac{\omega}{\Im}} \, q \int dr r^4 \rho(r) j_2(qr). \tag{2.18}$$

The $M3$ transition strength can be obtained by going to the photon point and results to be related to the $M1$ transition probability by

$$B(M3)\uparrow = 1.14 \delta^2 R^4 B(M1)\uparrow. \tag{2.19}$$

B. Experimental Evidence and Characterization of the Mode. A level with the properties of the $J^\pi = 1^+$, $K^\pi = 1^+$ state predicted by the TRM was discovered in a high resolution (e, e') experiment on ^{156}Gd by the group of Richter [1]. The $M1$ excitation was detected by performing (e, e') scattering at backward angles ($\theta = 165°$), where transverse magnetic transitions are dominant. The experimental form factor of this state is in close agreement with the TRM up to moderately high values of the momentum transfer q. The discrepancy at high q's is to be attributed to spin contributions, absent in the TRM [107,108].

Soon after, this strongly excited state was confirmed in (γ, γ') experiments [109]. In these reactions the decay of the $J^\pi = 1^+$ state to the $J^\pi = 2_1^+$ level of the ground state band was also observed. This allowed one to determine the K value of the state under investigation using the Alaga rule [110]. In fact in the rotational limit we have

$$R = \frac{B(M1, 1^+ \to 2_1^+)}{B(M1, 1^+ \to 0^+)} = \frac{|\langle 1K\lambda - K | 2\,0\rangle|^2}{|\langle 1K\lambda - K | 0\,0\rangle|^2}. \tag{2.20}$$

This ratio is $R = 0.5$ if $K = 1$, $R = 2$ if $K = 0$. Experimentally R is about 0.5 consistently with the $K = 1$ assignment.

Subsequent inelastic electron scattering and NRF experiments have ascertained the existence of the mode in three regions of the nuclear table, i.e., the deformed rare-earth nuclei [111—119], the fp-shell nuclei [120—122] and the actinides [123,124]. However, most of the experimental studies were performed on rare-earth nuclei.

We have pointed out already that the electron scattering form factors are in good agreement with the predictions based on the assumption that the excitation mode is of orbital nature. A further support to this property of the mode has been gained by comparing the (e, e') with the (p, p') scattering [120,125, 126]. In (p, p') reactions in fact, the intermediate energy proton scattering at small angles excites magnetic dipole states only through the spin part of the nucleon-nucleon interaction. The fact that the $M1$ states observed in electron scattering are not appreciably excited in the (p, p') reaction provides a strong evidence in favour of the orbital nature of the mode.

A combined analysis of (e, e') and (γ, γ') experiments [127] has shown that the mode is fragmented into several peaks closely packed around a prominent one with a total strength $B(M1)\uparrow \simeq 3\mu_N^2$. Attempts to clarify the nature of the single peaks have been made through (t, α) reactions [128,129].

Joint (e, e') and (γ, γ') experiments carried out on a chain of even Sm isotopes have shown that the integrated $M1$ strength grows quadratically with the deformation parameter [11] and is proportional to the strength of the $E2$ transition to the lowest 2^+ state [12]. The same deformation law was confirmed in Nd isotopes [13] and ascertained by now to hold for all nuclei of the rare-earth region [14,15]. The experiments on some actinides indicate that there is evidence for a δ^2 law also in this region [10,130]. This law is maybe the most spectacular manifestation of the scissors nature of the $M1$ transitions.

This systematic study was possible in virtue of the great progress made in gamma spectroscopy. Indeed, the measurement of the linear polarization of the scattered photons in nuclear resonance fluorescence (NRF) experiments has enabled parity assignment [17] and, thereby, the unambiguous identification of the $M1$ transitions [17—20]. The same experiments have ascertained the existence of $E1$ transitions intermixed with $M1$ excitations.

The experimental set-ups have now increased the detection sensitivity to a point that very weak transitions can be identified. A first success was the discovery of scissors-like excitations in γ-soft nuclei [131,132].

The present status of the experimental results can be found in several review articles [6—10]. The salient features of the mode which can be extracted from them are:

— The $M1$ strength is fragmented and distributed around an energy centroid, which assumes the value $\omega \simeq 3$ MeV in rare-earth nuclei.

— The summed strength in the most deformed rare-earth nuclei is $\Sigma B(M1)\uparrow \simeq 3\mu_N^2$.

— The transition is mainly promoted by the convection current. The orbital-to-spin ratio is typically $B_l(M1)/B_\sigma(M1) \simeq 10$.

— The integrated $M1$ strength depends quadratically on the deformation parameter and is strictly correlated with the strength of the $E2$ transition to the lowest 2^+ state.

While consistent with the observed properties of the mode on a qualitative ground, the TRM, in its original formulation [2], was unable to predict either the exact position of the energy centroid or the size of the total strength. Indeed, the TRM energy was higher than the observed one by about 1 MeV and the $M1$ strength was five times larger. The main reason of these strong discrepancies is to be found in the crude numerical estimates of the model parameters made in that paper. A rigid body moment of inertia was assumed and the restoring force constant was computed by paralleling the procedure adopted by Goldhaber and Teller for the $E1$ giant resonance. We know now that both prescriptions are unrealistic. There is however little doubt that the mode predicted by the model corresponds to the observed $M1$ excitations. We have already said that the experimental form factor is reproduced by the model to a large extent. We will see now that the model is also consistent with the quadratic deformation law.

C. Consistency of the TRM with the Deformation Law. As pointed out already, the most meaningful signature of the observed $M1$ transitions is the quadratic deformation law of the total $M1$ strength. It is therefore of the utmost importance to investigate if the TRM can predict such a behaviour. To this purpose it is useful to express all TRM quantities in terms of the shape variables $\alpha_{2\mu}$ instead of the angle ϑ and to impose for the proton (neutron) density (2.16) the normalization condition

$$\langle Q_{\lambda\mu}^{(\tau)} \rangle = \int \rho_\tau(\mathbf{r})\, r^\lambda Y_{\lambda\mu}(\mathbf{r})\, d\mathbf{r} = \alpha_{\lambda\mu}\, \rho_0^{(\tau)} R^{\lambda+3}, \tag{2.21}$$

where $\rho_0^{(p)}$ and $\rho_0^{(n)}$ are normalized to the number of protons and neutrons, respectively. Under a rotation by ϑ_τ ($\vartheta_p = \vartheta$, $\vartheta_n = -\vartheta$), around the x axis, the proton ($\tau = p$) and neutron ($\tau = n$) densities undergo the following change

$$\rho_\tau(R_{\vartheta_\tau}^{-1}\mathbf{r}) = \rho_\tau\left[r - R(1 + \sum_{\mu=\pm 1} \alpha_{2\mu}^{(\tau)} Y_{2\mu}^*(\hat{r})) \right], \tag{2.22}$$

where

$$\alpha_{2\mu}^{(\tau)} = D_{0\mu}^{(2)}(\vartheta_\tau)\, \alpha_{20}^{(\tau)} \simeq -i\sqrt{\frac{3}{2}}\, \alpha_{20}^{(\tau)} \vartheta_\tau = -i\sqrt{\frac{3}{2}}\, \beta_\tau \vartheta_\tau \tag{2.23}$$

to leading order in ϑ_τ. This key relation enables us to express the TRM Hamiltonian (2.3) in terms of shape variables, namely

$$H = \frac{1}{2\Im_{sc}} S^2 + \frac{1}{2} C_\vartheta \vartheta^2 = \frac{1}{2B_{sc}} \sum_{\mu=\pm 1} |\pi_{2\mu}|^2 + \frac{1}{2} C \sum_{\mu=\pm 1} |\alpha_{2\mu}|^2, \tag{2.24}$$

where $\pi_{2\mu}$ are conjugate to $\alpha_{2\mu}$ and

$$B_{sc} = \frac{4B_p B_n}{B_p + B_n}, \quad C = \frac{4C_p C_n}{C_p + C_n} \tag{2.25}$$

are the new model parameters. Old and new constants are related by

$$\Im_\tau = 3\beta_\tau^2 B_\tau, \quad C_\vartheta^{(\tau)} = 3\beta_\tau^2 C_\tau. \tag{2.26}$$

It follows from a simple inspection that, while the energy is independent of deformation, the scissors $M1$ strength grows quadratically with it. Indeed, upon insertion of the above expressions into the TRM harmonic relations (2.10), the scissors strength (2.11) becomes

$$B_{sc}(M1)\uparrow = \frac{9}{16\pi} B\omega\beta^2 g_r^2 \mu_N^2. \tag{2.27}$$

The δ^2 behaviour of the scissors $M1$ strength has been studied quantitatively in Ref.90 by making an empirical estimate of the mass parameter. The following expression was obtained

$$B_{sc}(M1)\uparrow \simeq 0.004\omega A^{5/3}\delta^2 g_r^2 \mu_N^2. \tag{2.28}$$

Numerical calculations carried out by putting $g_n = 0$ and $g_r = g_p = 2g_R = (2Z)/A$ yield results in good agreement with experiments [11—13]. In particular theoretical and experimental summed $M1$ strengths have similar saturation properties (Fig.1). A systematic analysis carried out recently [14,15] has shown that the $M1$ strengths computed by such an empirical formula are in overall agreement with experiments for all nuclei of the whole rare-earth region.

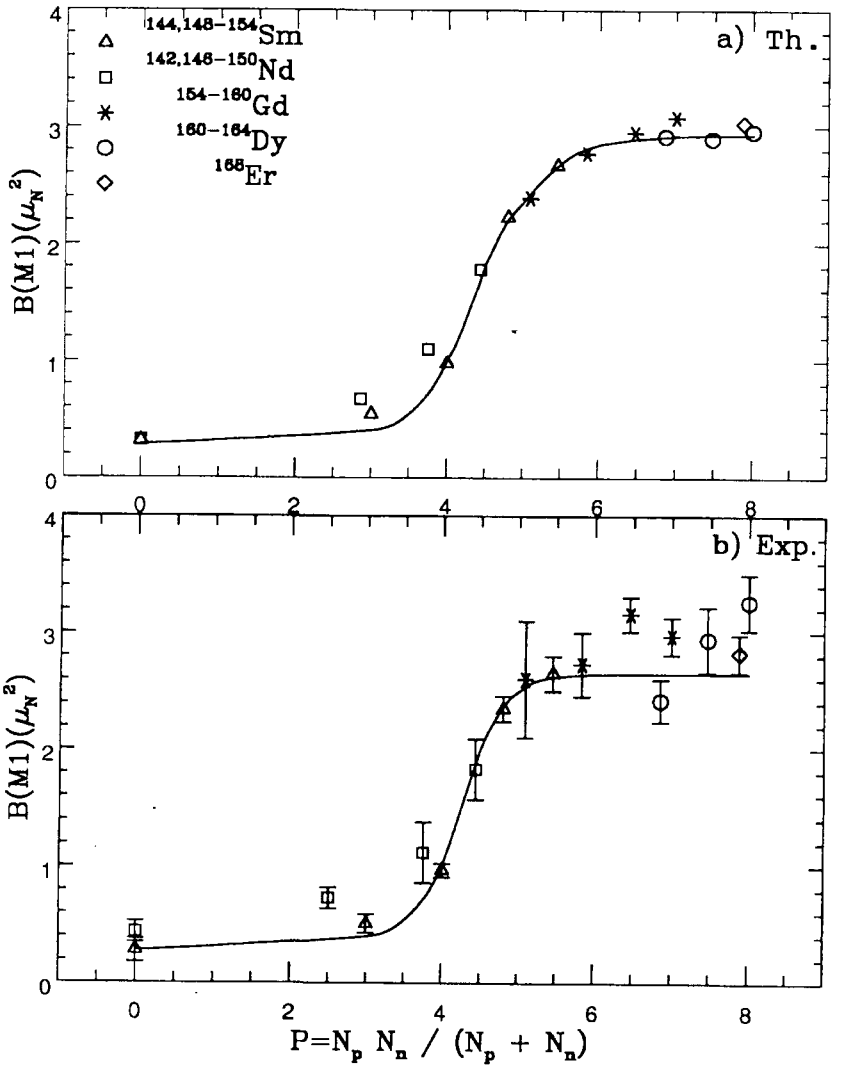

Fig.1. Saturation plot of the scissors $M1$ strength computed using the TRM formula (2.28). The quantity P is the Casten number defined in the text (eq. 3.32)

The formula has been shown to account also for the deformation dependence of the $M1$ strength in actinides isotopes [10,130] and in γ-soft nuclei [131,132].

D. Theoretical Computation of the TRM Constants: A Low and a High Energy Mode. *1. Classical Method.* Within the semiclassical domain one may attach to each of the two rotors the velocity fields

$$\upsilon_p = -\nabla\chi_p, \qquad \upsilon_n = -\nabla\chi_n, \tag{2.29}$$

where

$$\chi_\tau = \delta(x_{2_\tau} x_{3_\tau} \Omega_{1_\tau} + x_{1_\tau} x_{3_\tau} \Omega_{2_\tau}), \tag{2.30}$$

Ω_{i_τ} ($i_\tau = x_\tau, y_\tau$) are the proton and neutron angular velocities. One gets a two rotor Hamiltonian of the form given by eq. (2.1) and therefore an intrinsic one given by eq. (2.3) with an irrotational moment of inertia

$$\Im_{sc} = \Im_{irr} = \delta^2 \Im_{rig}, \qquad \Im_{rig} \simeq \frac{2}{5} mAR^2. \tag{2.31}$$

The restoring force constant can be deduced from the symmetry energy mass formula

$$\Delta V = \frac{1}{2} b_s \int \frac{(\delta\rho)^2}{\rho_0} d\mathbf{r} = \frac{1}{2} b_s \int \frac{(\delta\rho_p - \delta\rho_n)^2}{\rho_0} d\mathbf{r}, \tag{2.32}$$

where $b_s \simeq 50$ MeV and ρ_0 is the nuclear density normalized to the mass number. The density variation is computed by making use of eqs. (2.22) with the result

$$\delta_{\rho_\tau} = \rho_\tau(\vartheta_\tau) - \rho_\tau(0) = k_\tau \rho_0^{(\tau)} \sum_{\mu=\pm 1} \alpha_{2\mu}^{(\tau)} r^2 Y_{2\mu}^*, \tag{2.33}$$

where the constant k_τ is fixed by the normalization condition (2.21) and $\alpha_{2\mu}^{(\tau)}$ is given by eq. (2.32). The calculation of the integral in eq. (2.32) yields then

$$\Delta V = \frac{1}{2} C \vartheta^2, \tag{2.34}$$

where

$$C \simeq \frac{28}{5} b_s A \delta^2. \tag{2.35}$$

Using the above equations one gets for the energy of the mode and the corresponding strength (eq. (2.11))

$$\omega_+ \simeq 139.4 A^{-1/3} \text{ MeV}, \qquad B_+(M1) \uparrow \simeq 0.12 \delta^2 A^{4/3} g_r^2 \mu_N^2. \tag{2.36}$$

The strength is quadratic in the deformation parameter, but the energy is far higher than the observed one. We obtain indeed for ^{154}Sm $\omega \simeq 26$ MeV and $B(M1)\uparrow \simeq 4.7\mu_N^2$, having put $g_n = 0$ and $g_p = 2g_R = 2Z/A$. Although the $M1$ strength is reasonably close to the experimental value, the energy lies in the region of the giant isovector quadrupole resonance. What we have found is actually a new scissors mode. It is indeed the $K^\pi = 1^+$ component of the isovector quadrupole resonance mode. In order to obtain a low energy mode one has to make different assumptions about the nature of the rotors. A natural prescription for all possible alternatives can be found once the model is formulated in a microscopic context.

2. Microscopic Approach: Equivalence with Schematic RPA. Let us assume that nucleons move in a deformed mean field described by an anisotropic HO potential with frequencies ω_1 and ω_3 such that $\omega_1^2\omega_3 = \omega_0^3$ and $\omega_0 \simeq$ $\simeq 41A^{-1/3}$ MeV.

Mapping the procedure of Bohr and Mottelson unified theory [133] to the present case, one can make use of the harmonic relations (2.10) in the specific form

$$\frac{1}{\mathfrak{I}_{sc}}\langle S^2\rangle = \frac{1}{\mathfrak{I}_{sc}} \sum_{ph \in 2\omega_0} \sum_{\mu \pm 1} |\langle ph | S_\mu | \rangle|^2 = \omega_1 + \omega_3 \simeq 2\omega_0, \tag{2.37}$$

where $|\rangle$ is the particle-hole (p-h) vacuum. The sum is restricted to the $\Delta N = 2$p-h excitations. This condition yields the irrotational mass parameter

$$\mathfrak{I}_{sc} = \mathfrak{I}_{irr} = \delta^2 \mathfrak{I}_{rig}, \quad \mathfrak{I}_{rig} = \frac{1}{\delta\omega_0} \sum_{ph \in \delta\omega_0} |(S_+)_{ph}|^2 \simeq \frac{2}{5} mAR^2 \tag{2.38}$$

and the restoring force constant

$$C_0^{(+)} \simeq \mathfrak{I}_{irr}(2\omega_0)^2 \simeq \frac{28}{5} b_0 A\delta^2, \tag{2.39}$$

where $b_0 \simeq 17.5$ MeV. When the p-h interaction is switched on, the restoring force constant gets the additional contribution

$$C_1^{(+)} \simeq \frac{28}{5} b_1 A\delta^2, \tag{2.40}$$

where the constant b_1 follows from its relation to the energy symmetry potential $V_1 = 4b_1 \simeq 130$ MeV. The full restoring force constant $C_+ = C_0^{(+)} + C_1^{(+)}$ results to be exactly equal to the classical expression (2.35) with the same symmetry parameter $b_s = b_0 + b_1 \simeq 50$ MeV. It follows that the resulting energy and strength are given exactly by the semiclassical eqs. (2.36).

We use now eq. (2.10) with the following requirement

$$\frac{1}{\Im_{sc}}\langle S^2\rangle = \frac{1}{\Im_{sc}} \sum_{ph \in \delta\omega_0} \sum_{\mu=\pm 1} |\langle ph | S_\mu | \rangle|^2 \simeq \delta\omega_0, \tag{2.41}$$

where the sum is restricted to the $\Delta N = 0$ p-h space. This yields a rigid body moment of inertia $\Im_{sc} = \Im_{rig}$. The unperturbed restoring force constant is now

$$C_0^{(-)} \simeq (\delta\omega_0)^2 \Im_{rig} = \frac{28}{5} b_0^{(-)} A\delta^2 \tag{2.42}$$

with $b_0^{(-)} \simeq b_0/4$. The potential component can be fixed [133] from the ratio between the nuclear isovector and isoscalar average potential strengths V_1 and V_0, $a_- = C_1^{(-)}/C_0^{(-)} = b_1^{(-)}/b_0^{(-)} = -V_1/(4V_0) \simeq 0.6$. The final result is

$$\omega_- = \sqrt{\frac{C_-}{\Im_{rig}}} = \delta\omega_0\sqrt{1+a_-} \simeq 53\delta A^{-1/3}\ \text{MeV},$$

$$B_-(M1)\uparrow \simeq \frac{3}{4\pi}\Im_{rig}\omega_- \simeq 0.045\delta A^{4/3} g_r^2 \mu_N^2 . \tag{2.43}$$

The method just developed is nearly equivalent to the entirely classical one adopted in the TRM in its original formulation [2]. Both rely on the assumption that protons and neutrons form two rigid rotors. The present method however improves the computation of the restoring force constant with the result that the $M1$ strength is reduced by about a factor of two. Such a reduction however is not enough. In order to induce a further quenching, one needs to remove the rigid body assumption.

To this purpose one may impose for the low energy mode the alternative condition

$$\frac{1}{\Im_{sc}}\langle S^2\rangle = E(\varepsilon_{sp}) + E(\varepsilon_{sp} + \delta\omega_0), \tag{2.44}$$

where $E(\varepsilon_{sp}) = \sqrt{(\varepsilon_{sp} - \lambda)^2 + \Delta^2}$ is the quasiparticle energy. Here, ε_{sp} is the single particle (s.p.) energy referred to the chemical potential λ and Δ is the pairing gap. It is natural to use for λ the value $\lambda = (\delta\omega_0)/2$. With this choice the harmonic condition (2.10) becomes

$$\frac{1}{\Im_{sc}}\langle S^2\rangle = 2E = \sqrt{(\delta\omega_0)^2 + (2\Delta)^2}. \tag{2.45}$$

Using closure we obtain for the mass parameter

$$\Im_{sc} \simeq \Im_{sf} \simeq \frac{\delta\omega_0}{(2E)} (u(\varepsilon_{sp})\, v(\varepsilon_{sp} + \delta\omega_0) -$$

$$- (v(\varepsilon_{sp})\, u(\varepsilon_{sp} + \delta\omega_0))^2 \Im_{rig} \simeq \left(\frac{\delta\omega_0}{2E} \right)^3 \Im_{rig}, \tag{2.46}$$

having made use of the standard expressions of the BCS amplitudes u and v with $\lambda = (\delta\omega_0)/2$. The resulting energy and strength are

$$\omega_- = \sqrt{\frac{C_-}{\Im_{sf}}} \simeq (2E) \sqrt{1 + a_-},$$

$$B_-(M1)\uparrow \simeq \frac{3}{16\pi} \omega_- \Im_{rig} \left(\frac{\delta\omega_0}{2E} \right)^3 g_\tau^2 \mu_N^2 \tag{2.47}$$

or more explicitly

$$\omega_- \simeq 1.26(2\Delta) \sqrt{1 + x^2},$$

$$B_-(M1)\uparrow \simeq 0.001(2\Delta) A^{5/3} \frac{x^3}{1 + x^2} g_\tau^2 \mu_N^2, \tag{2.48}$$

where $x = \delta\omega_0/(2\Delta)$. According to these equations the strength goes like δ^3 for small deformations ($x << 1$) and becomes linear for very large deformations ($x >> 1$). In the range of observed deformations the strength is approximately quadratic in δ.

Had we averaged the two quasiparticle energies and the moment of inertia with respect to λ [133] we would have obtained exactly the strength derived by Hamamoto and Magnusson in schematic RPA [69]. This is not an accident. The approach presented here amounts exactly to a schematic RPA treatment. To show this equivalence we observe that, when expressed in terms of shape variables, the intrinsic TRM Hamiltonian (2.24) coincides with the harmonic Hamiltonian adopted within the unified theory [133]. Let us indeed switch from the normalization (2.21) to the new one

$$\langle Q_{\lambda\mu} \rangle = \int \rho(\mathbf{r}) r^\lambda Y_{\lambda\mu}(\mathbf{r})\, d\mathbf{r} = \alpha_{\lambda\mu}. \tag{2.49}$$

This induces in turn a renormalization of the mass and restoring force parameters which assume the new form

$$\Im_{sc} \Rightarrow B_\alpha = \frac{\Im_{sc}}{3\beta^2 \left(\frac{3}{4\pi} AR^2 \right)^2} = \frac{2\pi}{3} \frac{m}{AR^2},$$

$$C_\vartheta \Rightarrow C_\alpha = \frac{C}{3\beta^2 \left(\frac{3}{4\pi} AR^2 \right)^2} = C_\alpha^{(0)} + C_\alpha^{(1)}, \tag{2.50}$$

where

$$C_{\alpha}^{(0)} \simeq \frac{8\pi}{3}\frac{m\omega_0^2}{AR^2}, \quad C_{\alpha}^{(1)} \simeq \frac{7}{3}\frac{\pi V_1}{AR^4}. \tag{2.51}$$

The above quantities are just the mass parameters and coupling strengths derived within the unified theory approach [133].

The link with schematic RPA is now obtained simply through the standard mapping condition [133]

$$\sum_{\mu} |\alpha_{2\mu}|^2 = \sum_{\mu}\sum_{ph} |(Q_{2\mu}(1))_{ph}|^2, \quad Q_{2\mu}(1) = Q_{2\mu}^{(p)} - Q_{2\mu}^{(n)}. \tag{2.52}$$

Useless to say, an explicit RPA calculation yields exactly the results obtained here [34—36]. Although the deformation dependence is roughly reproduced, the magnitude of the strength produced by these calculations is about a factor of two larger than the experimental summed strength. A quenching mechanism is needed. This is hopefully found if the model can be framed in a fully microscopic context, which accounts also for spin degrees of freedom.

3. Scissors Modes in Superdeformed Nuclei. We have seen that, in its reformulated version, the TRM predicts a low and a high energy mode. In the first mode protons and neutrons behave approximately as superfluid systems, in the second as irrotational fluids. Being switched by deformation, the two modes should exist also in superdeformed nuclei. Their existence was indeed predicted in RPA [72] and within the classical TRM [134]. This latter model can be easily adapted to these nuclei. Let us indeed assume that K is a good quantum number so that the transition goes from K to $K+1$. The $M1$ operator couples the state $|IMK\rangle$ to the states $|I'M'K+1\rangle$ with $I' = I-1, I, I+1$. Using the standard expression for the transition matrix elements [133] with the TRM intrinsic wave function [2] and assuming $I >> K$ we obtain for the summed strength

$$\sum_{I'} B(M1, IK \to I'K+1) \simeq \frac{3}{16\pi}\Im_{sc}\,\omega\,\frac{1}{K+1}\,g_{\tau}^2\,\mu_N^2. \tag{2.53}$$

According to this expression the strength decreases with increasing K. If we assume that the superdeformed state has $K=0$, we gain the standard scissors expression (eq. 2.11). We may use eqs. (2.36) obtaining for the high energy mode of the superdeformed ^{152}Dy ($\delta \simeq 0.62$)

$$\omega_+ \simeq 26\ \text{MeV}, \quad B_+(M1)\uparrow \simeq 26.1\ \mu_N^2, \tag{2.54}$$

where we have put $g_n = 0$ and $g_p = 2g_R = 2Z/A$.

For the low energy mode we may assume rigid rotors and use eqs. (2.48) with $g_n = 0$ and $g_p = 1$, obtaining for the same superdeformed nucleus

$$\omega_- \simeq 6.1 \text{ MeV}, \quad B_-(M1)\uparrow \simeq 22.6\, \mu_N^2 . \tag{2.55}$$

The above numbers are in agreement with the RPA results of Ref. 72. They have been obtained under the assumption that, in going from deformed to superdeformed nuclei, protons and neutrons in their relative motion remain irrotational at high energy but undergo a transition from a superfluid to a rigid-body phase at low energy. Such an assumption is fully consistent with the conclusions drawn in Ref. 72.

We like to stress that, according to our equations based on the use of the TRM scissors wave function, these strong transitions occur only if the intrinsic superdeformed state has $K = 0$. If such a state has a nonvanishing but small K or contains K admixture, the corresponding strength should be still sizeable.

4. M1 Mode in Triaxial Nuclei. The model can be easily extended to triaxial nuclei [135,136]. To this purpose one can easily deduce the quadrupole fields entering into the $M1$ channel from the density variation induced by the rotation of protons against neutrons around each of the three principal axes. They are

$$Q_1 = -\frac{i}{\sqrt{2}} r^2 (Y_{21} + Y_{2-1})\, \tau_3 ,$$

$$Q_2 = -\frac{1}{\sqrt{2}} r^2 (Y_{21} - Y_{2-1})\, \tau_3 ,$$

$$Q_3 = \frac{-i}{\sqrt{2}} r^2 (Y_{22} - Y_{2-2})\, \tau_3 . \tag{2.56}$$

The corresponding excitation energies are

$$\varepsilon_1^{(\pm)} = |\omega_2 \pm \omega_3| = \omega_0 \left| e^{-\alpha \cos(\gamma - 4\pi/3)} \pm e^{-\alpha \cos \gamma} \right| ,$$

$$\varepsilon_2^{(\pm)} = |\omega_1 \pm \omega_3| = \omega_0 \left| e^{-\alpha \cos(\gamma - 2\pi/3)} \pm e^{-\alpha \cos \gamma} \right| ,$$

$$\varepsilon_3^{(\pm)} = |\omega_1 \pm \omega_2| = \omega_0 \left| e^{-\alpha \cos(\gamma - 2\pi/3)} \pm e^{-\alpha \cos \gamma (\gamma - 4\pi/3)} \right| . \tag{2.57}$$

The lowest eigenvalues for each mode are

$$\omega_i = \omega \cos \gamma \left(1 - \frac{(-1)^i}{\sqrt{3}} \operatorname{tg} \gamma \right), \quad i = 1, 2$$

$$\omega_3 = \frac{2}{\sqrt{3}} \omega \sin \gamma . \tag{2.58}$$

We have neglected pairing for simplicity.

The $E2$ and $M1$ strengths are

$$B_i(E2) = 1/2 \cos\gamma \left(1 - \frac{(-1)^i}{\sqrt{3}} \operatorname{tg}\gamma \right) B(E2), \quad i = 1, 2$$

$$B_3(E2) = \frac{2}{\sqrt{3}} \sin\gamma B(E2), \tag{2.59}$$

$$B_i(M1) = 1/2\cos\gamma \left(1 - \frac{(-1)^i}{\sqrt{3}} \operatorname{tg}\gamma \right) B(M1)$$

$$B_3(M1) = \frac{2}{\sqrt{3}} \sin\gamma B(M1). \tag{2.60}$$

For both kinds of transitions the ratio B_2/B_1 is

$$\frac{B_2}{B_1} = \frac{1 - \frac{1}{\sqrt{3}} \operatorname{tg}\gamma}{1 + \frac{1}{\sqrt{3}} \operatorname{tg}\gamma}. \tag{2.61}$$

A third mode, absent in axial nuclei, emerges. Its frequency and strengths contain γ as leading term consistently with the fact that such a mode disappears in the axial limit. For very small values of γ the frequency is very low and the strength is negligible.

According to the model predictions, a splitting of the $M1$ strength should signal a triaxial shape. Unfortunately such a splitting is likely to be hidden by the fragmentation induced by the nuclear shell structure. Such a test may therefore work only in some medium-light nuclei where the fragmentation induced by the shell structure can be modest.

E. Microscopic Formulation of the TRM. It is not obvious that the scissors picture should be preserved within a microscopic context. The spin degree of freedom can in fact interfere so as to destroy such a picture. This is to be expected to some extent since the spin orbit coupling induces a large fragmentation in the s.p. spectrum. In order to check if the scissors picture still holds, it is useful to analyse the excitation mechanism. The full shell model $M1$ operator is

$$\mathcal{M}(M1, \mu) = \sqrt{3/(4\pi}} \sum_{i=1}^{A} (g_l(i)\, l_\mu(i) + g_s(i)\, s_\mu(i))\, \mu_N. \tag{2.62}$$

The scissors picture remains valid only if the spin contribution is negligible or can be absorbed into the generator S so that the $M1$ operator can be written in the TRM form

$$\mathcal{M}(M1, \mu = 1) = \left(\frac{3}{16\pi} \right)^{1/2} S_{+1}(g_p - g_n)\, \mu_N \,. \tag{2.63}$$

In such a case general definitions of the TRM constants valid in any microscopic context can be given easily. To this purpose it is useful to write the defining TRM eq. (2.10) in the form [34]

$$\Im_{sc} = \sum_{\mu = \pm 1} \langle 0 | S_\mu^\dagger \frac{1}{H - E_0} S_\mu | 0 \rangle,$$

$$C = \frac{1}{2} \sum_{\mu = \pm 1} \langle 0 | [S_\mu^\dagger, [H, S_\mu]] | 0 \rangle. \tag{2.64}$$

Using closure one obtains the quite general expressions

$$\Im_{sc} = \sum_{n\mu} \frac{1}{\omega_n} | \langle n\mu | S_\mu | 0 \rangle |^2,$$

$$C = \sum_{n\mu} \omega_n | \langle n\mu | S_\mu | 0 \rangle |^2. \tag{2.65}$$

It is now immediate to derive the scissors energy weighted $M1$ sum rule

$$\sum_n \omega_n B_n(M1)\uparrow = \frac{3}{16\pi} \sum_{n,\tau} \omega_n | \langle n\mu | S_\mu | 0 \rangle |^2 g_\tau^2 \mu_N^2 =$$

$$= \frac{3}{32\pi} \sum_{\mu = \pm 1} \langle 0 | [S_\mu^\dagger, [H, S_\mu]] | 0 \rangle g_\tau^2 \mu_N^2 \simeq \frac{3}{16\pi} \Im_{sc}\, \omega^2 g_\tau^2 \mu_N^2 \,. \tag{2.66}$$

This sum rule holds in the macroscopic as well as in the microscopic domain. Under the experimentally supported assumption of small fragmentation of the mode, we obtain for the summed strength the expression defining the TRM $M1$ strength (eq. 2.9). It follows that the TRM formula, with $\Im_{sc}$ and C given by eq.(2.65), represents a general definition of the scissors $M1$ summed strength. Microscopic studies of these formulas have been carried out in Ref. 137.

3. BOSON MODEL DESCRIPTIONS

The TRM was formulated specifically for identifying a collective mode of scissors nature and predicting its signature. Hence the simplifying assumption that neutrons and protons form two fluids of ellipsoidal shape. On the other hand, the mode can be fully understood only if studied in more realistic

approaches which include additional degrees of freedom. An obvious extension consists in allowing for surface vibrations of proton and neutron deformed fluids. This is accomplished within a semiclassical context by describing these vibrations in terms of the shape variables α_p and α_n. These are indeed the classical variables adopted in the phenomenological models described in this section.

A. Extended Bohr–Mottelson Models. The TRM Hamiltonian, when written in terms of the Bohr–Mottelson collective variables (2.24), assumes the form adopted by Faessler and coworkers [30] to study the mode. In their approach the TRM Hamiltonian was derived from the proton-neutron Hamiltonian introduced within the extended Bohr–Mottelson model developed by Faessler himself to describe the $E2$ giant resonances [138]. The novelty of this model consisted in the introduction of collective variables for protons (α_p) and neutrons (α_n). Nuclear and relative motions could then be decoupled by defining the new variables

$$\alpha_\mu = \frac{1}{2}(\alpha_\mu^p + \alpha_\mu^n), \qquad \xi_\mu = \alpha_\mu^p - \alpha_\mu^n . \tag{3.1}$$

The α_μ coordinates are quadrupole shape variables describing the motion of the nucleus as a whole, while ξ_μ account for the relative motion between the proton and neutron fluids.

In their study of the scissors mode [30], the authors started from an Hamiltonian of the form (2.24) and by using a relation similar to the one given by eq.(2.23) gain a TRM Hamiltonian of the form (2.3). They improved the rigid TRM results [2] by assuming that the motion is determined by a fraction of nucleons only. Because of this ansatz, moment of inertia and restoring force constant are reduced by about a factor of three. Their $M1$ strength resulted to be only twice the observed one.

The same formalism was adopted by Rohozinski and Greiner [31] in a more extended frame. They in fact formulated the problem in the laboratory frame using a highly anharmonic Hamiltonian in the variables α_μ and ξ_μ. For small amplitude oscillations the Hamiltonian can be decomposed into

$$H = H_{\text{coll}}(\alpha) + H_{\text{rel}}(\xi) + H_{\text{int}}(\alpha, \xi), \tag{3.2}$$

where H_{coll} describes the mass collective motion, H_{rel} is an harmonic Hamiltonian in the relative coordinates ξ_μ and H_{int} is an interaction term which couples the two motions.

A similar decomposition holds for the total angular momentum

$$L_{1\mu} = L^n_{1\mu}(\alpha_n) + L^p_{1\mu}(\alpha_p) = L^{\text{coll}}_{1\mu}(\alpha) + L^{\text{rel}}_{1\mu}(\xi). \tag{3.3}$$

Transforming to the intrinsic frame defined by the principal axes of the system, the variables α_μ are turned into the Euler angles (α, β, γ) and the intrinsic shape variables a_{20} and a_{21}, while the transformed relative coordinates ξ_μ remain still five in number. In the strong coupling limit one can put in the interaction term the equilibrium values appropriate for an axially symmetric shape, namely $a_{20} = \beta$ and $a_{22} = 0$. In this limit the transformed Hamiltonian becomes

$$H = H_{\text{rot}} + H_{\beta\gamma} + H_{\text{centr}} + H_{\text{coriolis}} + H_{\text{sc}}\,. \tag{3.4}$$

H_{rot} and $H_{\beta\gamma}$, describing respectively the nuclear rotation and the β and γ vibrations around an equilibrium spheroidal shape of deformation β, form essentially the Bohr Hamiltonian [133], while H_{centr} and H_{coriolis} are the centrifugal and Coriolis terms. The last piece is the scissors Hamiltonian. This, in the strong coupling limit, can be written

$$H_{\text{sc}} = H_{\text{rel}}(\xi) + H_{\text{int}}(\xi, \beta) = \sum_{K=0}^{2} H_K\,, \tag{3.5}$$

where H_K are HO Hamiltonians in the relative coordinates and carry intrinsic angular momenta $K = 0, 1, 2$. The coupling between the relative motion and the mass deformation mode induces a dependence of the restoring force constant C_K and the mass parameter B_K on K and β.

The NPD model predicts therefore two other isovector modes in addition to the scissors excitation. The magnetic orbital dipole form-factor operator is obtained from the general expression (2.14) assuming an irrotational velocity field and a proton mass density of the form (2.16). The resulting expression is

$$T^{(m)}_{1\mu} = \frac{i}{\sqrt{2m}} \sqrt{\frac{3}{4\pi}}\, F(q)\, L^p_{1\mu} \tag{3.6}$$

with

$$F(q) = \frac{\int_0^\infty r^3\, dr \left[j_1(qr) + \frac{qr}{5} j_2(qr) \right] f'(r - R_0)}{\int_0^\infty r^3\, dr\, f'(r - R_0)}\,. \tag{3.7}$$

The $M1$ strength is obtained by going to the photon point and results to be of the same TRM form (2.11) with an irrotational moment of inertia. The NPD

model describes therefore the mode as a rotational oscillation between two irrotational fluids.

The advantage of this model consists in that it describes on equal footing the scissors as well as the β and γ vibrations and accounts for the coupling between them. The model, however, does not give clear and simple prescriptions for computing the parameters. These are in practice determined by a fit to the energy and the $B(M1)$ values. Another drawback is the lack of agreement between model and experimental form factors.

The model was extended so as to enable the study of the effect of triaxial deformation on the $M1$ strength [139]. It was found that, contrary to the TRM, a small triaxiality does not lead to the appearance of 1^+doublets.

B. Generalized Coherent State Model Description. The anharmonic terms of the NPD Hamiltonian are not ease to handle. An efficient approach for dealing with is provided by the so-called coherent state model (CSM) [140].

The idea of the CSM is to describe the low-lying collective states of spherical as well as deformed nuclei by wave functions obtained through angular momentum projection from intrinsic coherent states, which represent a quadrupole boson condensate. The second step consists in constructing an effective interacting boson Hamiltonian which is diagonal in the above states to a large extent. As in the NPD model the CSM Hamiltonian is anharmonic and does not preserve the number of bosons. Because of the use of coherent states, however, such a Hamiltonian is of the simplest form. This model has been used successfully to describe the collective properties of nuclei from the spherical to the transitional and deformed regions.

The $M1$ mode can be studied in its generalized version (GCSM) [32,33], where distinction is made between neutron and proton bosons. The structure of the generic GCSM state is

$$\Psi_{\alpha JMK} = N_{\alpha J} P^J_{MK} \varphi_{\alpha K}, \tag{3.8}$$

where $N_{\alpha J}$ is a normalization constant, P^J_{MK} is a projection operator of standard form which projects the good angular momentum out of the intrinsic states $\varphi_{\alpha K}$. These are obtained by acting with boson operators, at most quadratic in the quadrupole creation operators $b^+_{\tau\mu}$, on a HO coherent state in the deformation parameters d_p and d_n

$$\varphi_0 = \exp\left[d_p(b^+_{p0} - b_{p0}) - d_n(b^+_{n0} - b_{n0})\right] |\rangle. \tag{3.9}$$

States describing one β band, two γ bands and two $K^{\pi} = 1^{+}$ bands have been constructed. The one describing the scissors mode band is

$$\Psi_{JM1} = N_1^J P_{M1}^J (b_p^+ \otimes b_n^+)_{11} |0\rangle. \tag{3.10}$$

The Hamiltonian is constructed so as to be diagonal to a good approximation in the bands of the six boson states. Its expression is

$$H = A_1(n_p + n_n) + A_2(n_{pn} + n_{np}) +$$

$$+ \sqrt{5}\,\frac{A_1 + A_2}{2}\,(P_n^+ + P_{np}^+ + A_3(P_p^+ P_n + P_n^+ P_p - 2P_{np}^+ P_{np}) + A_4 J^2, \tag{3.11}$$

where n_p and n_n are the proton and neutron number operators and together with n_{pn} and n_{np} can be written in the compact form

$$n_{kk'} = \sum_{\mu} b_{k\mu}^+ b_{k'\mu}, \qquad k = p, n; \qquad k' = p, n, \tag{3.12}$$

P_p^+, P_n^+ and P_{np}^+ are proton, neutron and proton-neutron pairing-like boson operators

$$P_{kk'}^+ = (b_k^+ b_{k'}^+)_0 - d^2/\sqrt{5} \tag{3.13}$$

and the quantities A_i, $i = 1, 4$ are free adjustable parameters.

Eq.(3.11) defines an interacting boson Hamiltonian which does not commute with the boson number operators n_p and n_n. Its excitation energies are obtained as

$$\omega = \langle \Psi_{1M} | H | \Psi_{1M} \rangle - \langle \Psi_0 | H | \Psi_0 \rangle. \tag{3.14}$$

The parameters A_i are determined from fitting some levels of the ground, β and γ bands while the deformation parameter, assumed equal for protons and neutrons, is fixed by an overall fit of the β band. The only free parameter is the scaling parameter entering into the canonical transformation

$$\alpha_{\tau\mu} = \frac{1}{\sqrt{2}\,k_\tau}\,(b_\mu^+ + b_{\bar{\mu}}). \tag{3.15}$$

In the harmonic limit, this parameter assumes the standard form $k_\tau = \sqrt{B_\tau C_\tau}$.

The $M1$ operator has been derived from the general expression (2.14) using an irrotational velocity field (eq. 2.29) and a charge density of the form (2.16) as in the NPD model. The resulting expression to lowest order is

$$T(M1, \mu) = -iej_1(qR_0)(g_p J_{p\mu} + g_n J_{n\mu}), \tag{3.16}$$

where $J_{k,\mu} = \sqrt{10}(b_k^+ b_k)_{1\mu}$. By going to the photon point, it is possible to obtain for the $M1$ strength a rotational and a vibrational limit [89]

$$B_{\text{rot}}(M1)\uparrow = \frac{9}{4\pi} k_p^2 \beta^2 g_{\text{rel}}^2 \mu_N^2,$$

$$B_{\text{vib}}(M1)\uparrow = \frac{18}{\pi} k_p^2 \beta^2 g_{\text{rel}}^2 \mu_N^2. \tag{3.17}$$

This value is linear in β^2 in both cases but with two different slopes. The full GCSM expression was used to compute the $M1$ strength for different chains of isotopes. The experimental δ^2 behaviour was nicely reproduced. If we put $k_p^2 = B\omega$, valid in the harmonic approximation, we obtain for the strength in the rotational limit the TRM expression (2.27). The close link between the two approaches was discussed in Ref. 89.

The $M1$ form factor was computed in plane wave approximation [143]. Although a detailed comparison with experiments cannot be carried out, it looks promisingly close to the observed one. The octupole operator has exactly the same expression of the $M1$ operator with a gyromagnetic ratio $g_{p/n}^{(3)} = 12/7 g_{p/n}$. Once the magnetic dipole gyromagnetic ratios are determined, the octupole ones are automatically fixed. The model predicts a scissors, an isoscalar and an isovector $M3$ transitions [141]. The isoscalar $M3$ strength is remarkably close to the one measured in ^{164}Dy and consistently interpreted as isoscalar [142].

The GCSM has also been extended to triaxal nuclei [143]. The results obtained are consistent with the TRM findings.

C. Algebraic Description of the Mode: The Interacting Boson Model. *1. The model.* The basic assumption of the interacting boson model [144,145] is that the low-lying collective states of nuclei away from major closed shells are described in terms of a monopole boson with angular momentum and parity $J^\pi = 0^+$, called s boson, and a quadrupole boson with $J^\pi = 2^+$, called d boson. These s and d bosons are interpreted as strongly correlated pairs of valence nucleons coupled respectively to $J^\pi = 0^+$ and $J^\pi = 2^+$.

In the first formulation of the model (IBM1) no distinction is made between protons and neutrons. The Hamiltonian has the form

$$H_B = E_0 + \sum_{\alpha\beta} \varepsilon_{\alpha\beta} B^+_\alpha b_\beta + \frac{1}{2} \sum_{\alpha\beta\gamma\delta} u_{\alpha\beta\gamma\delta} b^+_\alpha b^+_\beta b_\delta b_\gamma, \tag{3.18}$$

where E_0 is a c number, $\varepsilon_{\alpha\beta}$ and $u_{\alpha\beta\gamma\delta}$ are the free parameters, b^+_α and b_α are respectively the creation and destruction (s or d) boson operators. The distinguishing property of this boson Hamiltonian is that it contains in addition to the harmonic term a two-body part and commutes with the total number of bosons. Moreover it has a definite group structure since the bilinear products are the 36 generators of the group $U(6)$. This allows one to find the proper basis states for its diagonalization. In fact, one can generate from $U(6)$ three subgroup chains containing the rotation group as a subgroup. These are

$$U(6) \supset \begin{cases} U(5) \supset 0(5) \supset 0(3) \supset 0(2) & \text{I} \\ \rightarrow SU(3) \supset 0(3) \supset 0(2) & \text{II} \\ 0(6) \supset 0(3) \supset 0(2) & \text{III} \end{cases} \tag{3.19}$$

Each group chain provides the quantum number for labeling a set of basis states.

The boson Hamiltonian, in its general form, can be diagonalized in one of these bases only numerically. For an appropriate choice of the parameters, however, it can be written as a sum of linear and quadratic Casimir invariants of one of the three chains. In these limiting cases the eigenvalue problem can be solved algebraically.

The states obtained in these three limits can be interpreted geometrically by making use of the concept of coherent states. It can be shown that in the chain I the states describe the vibrational motions of spherical nuclei, chain II corresponds to an axially symmetric rotor and chain III to γ-unstable rotor.

In the second version of the interacting boson model (IBM2) one makes distinction between neutrons and protons and assumes that the low-lying levels of nuclei can be explained in terms of pairs of protons and pairs of neutrons with $J^\pi = 0^+$ and $J^\pi = 2^+$, treated as s_π d_π and s_ν d_ν bosons.

In order to take into account the p-h conjugation in particle space, the number of protons, N_π, and the number of neutrons, N_ν, is counted from the nearest closed shell.

The Hamiltonian for the coupled system of proton and neutron bosons can be written as

$$H = H_\pi + H_\nu + V_{\pi\nu}, \tag{3.20}$$

where $H_\pi(H_\nu)$ are the proton (neutron) boson Hamiltonian of the form (3.18) and $V_{\pi\nu}$ is the proton-neutron boson interaction. Also the IBM2 has a group structure, that of the group product $U_\pi(6) \otimes U_\nu(6)$. One can generate from this

group several group chains containing the rotation group as a subgroup, each one leading to a definite classical limit.

The chain leading to the scissors mode is the following

$$U_\pi(6) \otimes U_\nu(6) \supset U_{(\pi+\nu)}(6) \supset SU_{(\pi+\nu)}(3) \supset 0(3) \supset 0(2). \tag{3.21}$$

Since the proton and neutron bosons are nonidentical, from the tensor product of the two $U(6)$ symmetric representations one generates symmetric as well as mixed symmetry representations. In order to label the states of different $U_{\pi+\nu}(6)$ symmetry it has become customary to introduce a new quantum number, called the F spin, formally equivalent to isospin for particles. A proton boson has $F = 1/2$ and third component $F_3 = +1/2$, a neutron boson has $F = 1/2$ and $F_3 = -1/2$. For a system of $N = N_\pi + N_\nu$ bosons, the totally symmetric states have maximum F spin, $F = F_{mx} = (N_\pi + N_\nu)/2$, the states with mixed symmetry have $F = F_{mx} - 1$, etc.

The most general IBM2 Hamiltonian has too many parameters to be of any practical use. A schematic Hamiltonian frequently used is of the form

$$H = \varepsilon(n_{d\pi} + n_{d\nu}) + 2K_{\pi\nu}Q_\nu \cdot Q_\pi + K_{\nu\nu}Q_\nu \cdot Q_\nu + K_{\pi\pi}Q_\pi \cdot Q_\pi + \lambda M, \tag{3.22}$$

where $n_{d\pi}$ and $n_{d\nu}$ are the proton and neutron $J^\pi = 2^+$ number operators, Q_π and Q_ν are the proton and neutron quadrupole operators and M is the so-called Majorana operator related to the Casimir invariant of the group $U_{\pi+\nu}(6)$ and is responsible for the splitting between totally symmetric and mixed symmetry representations.

In the special case $\varepsilon = 0$, and $K_{\pi\nu} = K_{\pi\pi} = K_{\nu\nu} = K$, the Hamiltonian (3.22) can be expressed as the sum of the Casimir invariants of the group chain (3.21) and is therefore diagonal in this scheme. The energy spectrum can be calculated algebraically. One obtains symmetric as well as mixed-symmetry bands, where $J^\pi = 1^+$ levels appear.

The first excited $J^\pi = 1^+$ state describes the scissors mode [4]. Due to the lack of experimental information on other mixed symmetry levels, the Majorana parameter is fixed by fitting the observed energy of this $J^\pi = 1^+$ state. The IBM cannot therefore predict the energy of the scissors mode.

The $M1$ operator has the form

$$\mathcal{M}(M1) = \sqrt{\frac{3}{4\pi}}\,(g_\pi L_\pi + g_\nu L_\nu)\,\mu_N = \mathcal{M}_s + \mathcal{M}_\upsilon, \tag{3.23}$$

where the F spin scalar and vector components are

$$\mathcal{M}_s(M1), \mu) = \sqrt{\frac{3}{4\pi}}\, g_R\, L_\mu\, \mu_N = \sqrt{\frac{3}{4\pi}}\, g_R (L_{\pi,\mu} + L_{\nu,\mu})\, \mu_N , \tag{3.24}$$

$$\mathcal{M}_v(M1, \mu) = \sqrt{\frac{3}{4\pi}}\, (g_\pi - g_\nu) \left(\frac{N_\nu}{N} L_{\pi,\mu} - \frac{N_\pi}{N} L_{\nu,\mu} \right) \mu_N \tag{3.25}$$

and the gyromagnetic factor is obtained from the F spin scalar term

$$g_R = \frac{\langle \mu \rangle}{L} = \frac{g_\pi \langle L_\pi \rangle + g_\nu \langle L_\nu \rangle}{\langle L \rangle} = \frac{g_\pi N_\pi + g_\nu N_\nu}{N} . \tag{3.26}$$

The g_π and g_ν factors can be computed microscopically by following a boson-fermion mapping procedure [146]. Since the underlying idea in IBM is that the s and d bosons represent strongly correlated $J^\pi = 0^+$ and $J^\pi = 2^+$ nucleon pairs, one can turn the boson state Ψ_B into a fermion state Ψ_F by substituting the boson operators s^+ and d^+ with correlated fermion pair operators

$$S^+ = \sum_i c_i^{(0)} (a_i^+ a_i^+)_0^0 , \quad D_\mu^+ = \sum_{ij} c_{ij}^{(2)} (a_i^+ a_j^+)_\mu^2 . \tag{3.27}$$

The boson operator O_B is then defined by equating the matrix elements

$$\langle \Psi_B | O_B | \Psi'_B \rangle = \langle \Psi_F | O_F | \Psi'_F \rangle , \tag{3.28}$$

where O_F is the shell-model operator.

The microscopic estimates based on the above procedure give [147,148] $g_\pi \cong 1$ and $g_\nu \cong 0$. Alternatively they can be estimated empirically from the comparison with the experimental g factor of the 2^+ states [29,149,150]. The values so determined can deviate from $g_\pi \cong 0$ and $g_\nu \cong 0$ by 25—30%.

The F spin vector term couples the ground state to the $J^\pi = 1^+$ mixed symmetry state of the scissors mode with a strength given by [4,29,148]

$$B(M1) = \frac{3}{4\pi} \frac{8 N_\pi N_\nu}{2N - 1} (g_\pi - g_\nu)^2 \mu_N^2 . \tag{3.29}$$

It is to be noticed that only valence nucleons contribute to the strength. Using the values $g_\pi = 1$ and $g_\nu = 0$ for ^{156}Gd, $N_\pi = 7$ and $N_\nu = 5$, one obtains $B(M1) \cong 2.8\, \mu_N^2$, a value remarkably close to experiments.

The IBM form factor is computed by using the microscopic expression of the s and d bosons. It contains therefore some spin contribution. Its agreement with experiments is satisfactory even at high momentum transfers, where the spin term is dominant and where the TRM appears clearly to be inadequate [107,108]. These results have been confirmed in subsequent calculations [151,152]

The IBM description of the mode is on the other hand closely related to the TRM. As we will see, in the classical limit the IBM Hamiltonian assumes indeed the TRM form.

The $M3$ operator has a similar structure

$$\mathcal{M}(M3) = \sqrt{\frac{35}{8\pi}} \, (g_\pi^{(3)} (d_\pi^+ d_\pi)_{3\nu} + g_\nu^{(3)} (d_\nu^+ d_\nu)_{3\nu}), \tag{3.30}$$

where, for the lack of experimental data, the gyromagnetic ratios are to be determined microscopically by a boson-fermion mapping procedure similar to the one sketched for the $M1$ case. The model predicts [24] three $M3$ transitions, one F spin symmetric and two of mixed symmetry including the scissor mode. Numerically [24,29] the mixed symmetry transition strengths resulted quite strong ($B(M3)\uparrow \simeq 0.35 \div 0.6 \, \mu_N^2 \, b^2$), while the symmetric strength comes out to be too weak ($B(M3)\uparrow \simeq 0.09 \, \mu_N^2 \, b^2$), with respect to the experimental value [142] ($B(M3)\uparrow \simeq 0.3 \, \mu_N^2 \, b^2$.

2. Connection with the TRM and Deformation Law. The $M1$ strength given by eq. (3.29) is valid in the $SU(3)$ limit. The most general IBM2 summed $M1$ strength consistent with the conservation of F spin symmetry is [84]

$$B(M1)\uparrow = \frac{3}{16\pi} \langle 0 | S^2 | 0 \rangle (g_\pi - g_\nu)^2 \, \mu_N^2 \simeq$$

$$\simeq \frac{9}{4\pi} P \frac{\langle N_d \rangle}{N-1} (g_\pi - g_\nu)^2 \, \mu_N^2 , \tag{3.31}$$

where N_π and N_ν denote the number of valence proton and neutron pairs respectively, $N = N_\pi + N_\nu$, $\langle N_d \rangle$ is the average number of quadrupole bosons in the ground state; and P, the fractional number introduced by Casten [153]

$$P = 2 \frac{N_\pi N_\nu}{N} . \tag{3.32}$$

The IBM2 $M1$ strength in the $SU(3)$ limit is obtained as a special case by putting $n_d = \langle N_d \rangle / N = 2/3$.

One can derive a semiclassical expression of the IBM2 strength by the following procedure [92]. Let us write

$$N_d = N_d^{(p)} + N_d^{(n)} = d_p^\dagger \cdot d_p + d_n^\dagger \cdot d_n, \tag{3.33}$$

having denoted by $d_\tau^\dagger$ and d_τ the quadrupole boson creation and annihilation operators, respectively. Being a scalar, N_d can be referred to the intrinsic frame. In the classical limit, the harmonic approximation holds. We can then transform to shape variables by means of the canonical transformation

$$\alpha_{2\mu}^{(\tau)} = \alpha_0^{(\tau)}(d_{\tau,\mu}^\dagger + d_{\tau,\mu}), \qquad \alpha_0^{(\tau)} = \sqrt{\frac{1}{2B_\tau \omega}}. \tag{3.34}$$

The $\mu = 1$ components are the shape scissors variables. We can therefore assume ω to be the energy of the scissors mode.

In dealing with an axially symmetric system it is appropriate to take as intrinsic ground state a HO wave function which is coherent only in the proton and neutron $\mu = 0$ components of $\alpha_{2\mu}^{(\tau)}$. We have

$$\begin{aligned} d_{\tau,0}\,\psi_c &= d'_\tau \psi_c \\ d_{\tau,\mu}\,\psi_c &= 0, \qquad (\mu \neq 0), \end{aligned} \tag{3.35}$$

where d'_τ are pure c numbers. It follows that

$$\beta_\tau = \langle\, \alpha_{20}^{(\tau)} \,\rangle_c = 2\alpha_0^{(\tau)} d'_\tau. \tag{3.36}$$

In the strong coupling limit we then obtain

$$\begin{aligned} \langle N_d \rangle &= \frac{1}{4}\left[\left(\frac{\beta_p}{\alpha_0^{(p)}}\right)^2 + \left(\frac{\beta_n}{\alpha_0^{(n)}}\right)^2\right] = \\ &= \frac{1}{2}\,\omega(B_p\,\beta_p^2 + B_n\,\beta_n^2) \simeq \frac{1}{2}\,\omega B \beta^2. \end{aligned} \tag{3.37}$$

The above equation shows that the number of quadrupole bosons in the IBM2 ground state is strictly correlated with the Bohr–Mottelson deformation parameter β. The link between the $M1$ strength and deformation is equally close. Indeed upon insertion in eq. (3.31) we get

$$B^{(cl)}(M1)\uparrow \simeq \frac{9}{8\pi}\,\frac{P}{N-1}\,\omega B \beta^2 (g_\pi - g_\nu)^2\,\mu_N^2. \tag{3.38}$$

In virtue of this relation, the IBM2 strength appears to be quadratic in the deformation parameter consistently with experiments. Such a property is hidden

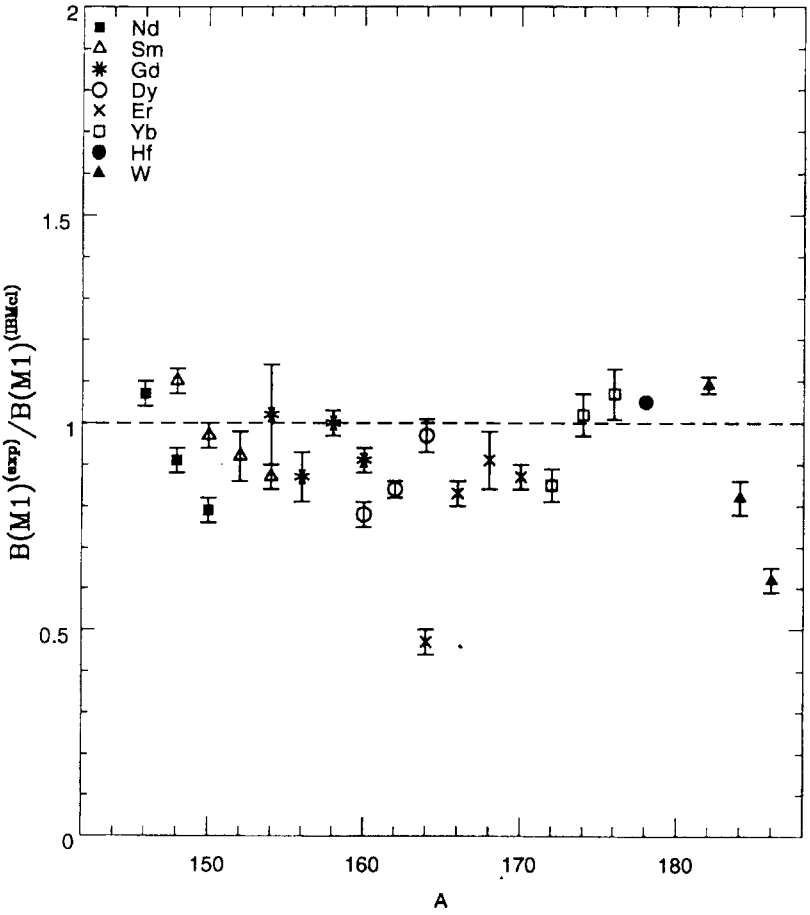

Fig.2. Ratio between the IBM $M1$ strength computed in the semiclassical limit (eq. 3.38) and the experimental value in the rare-earth region

when the same strength is expressed in the IBM2 formalism. Figure 2 shows that in the classical limit of IBM2 the experimental trend of the $M1$ strength is closely reproduced. Another method for deriving the classical limit of the same IBM $M1$ strength (3.31) has been developed in Ref. 91. The results obtained are of the same quality.

3. The TRM as Geometric Limit of the IBM2: Explicit Derivation. The close link of the IBM2 approach with the TRM was explicitly proved [154—157]. Using coherent states of the form

$$|\Psi_\alpha\rangle = \exp\left(\sum_{k=\pi,\nu}(\alpha_{sk}\, s_k^+ + \alpha_{dk}\cdot d_k^+)\right)|0\rangle \tag{3.39}$$

the IBM Hamiltonian is turned into a classical one

$$H(\alpha_{sk}, \alpha_k, \alpha_{sk}^*, \alpha_k^*) = \langle \Psi_\alpha | H_B | \Psi_\alpha \rangle, \qquad k = p, n. \tag{3.40}$$

Because of the conservation of the total number of bosons N, α_{sk} can be expressed in terms of N and α_k. The resulting Hamiltonian depends on ten coordinates α_p and α_n, five for protons and five for neutrons, and their complex conjugates, as in the two-boson models illustrated previously.

The link of the IBM as well as of the other boson model with the TRM can be established by the following procedure.

One can transform these shape coordinates α_k into the intrinsic coordinates β_k and γ_k and the Euler angles $(\alpha\beta\gamma)$ by the canonical transformation

$$\alpha_{k,\mu} = \sum_\nu a_{k,\nu} D^{(2)}_{\mu\nu}(\Omega_k) \tag{3.41}$$

and similarly for the conjugate momenta π_k. In the above equation $a_{k,\mu}$ have the expressions

$$a_{k,0} = \beta_k \cos\gamma_k,$$
$$a_{k,\pm 2} = \frac{1}{\sqrt{2}}\beta_k \sin\gamma_k,$$
$$a_{k,\pm 1} = 0. \tag{3.42}$$

In IBM the deformation parameter γ is equal to the Bohr and Mottelson corresponding quantity, while the parameter β is a function of the parameter β of Bohr and Mottelson.

In order to derive the Hamiltonian describing the scissors mode one must freeze the shape variables by putting their equilibrium values. For an axially symmetric system one has $\gamma_\pi = \gamma_\nu = 0$, while the values of β are obtained by minimizing the energy. Of the two sets of Euler angles $(\Omega = \alpha\beta\gamma)$, the angles γ's are redundant if we impose $L_3^\pi = L_3^\nu = 0$ consistently with the assumption of axial symmetry. The remaining angles can be transformed to an angle θ between the symmetry axes and to a set of Euler angles describing the orientation of the full system, exactly as in the TRM. This program was carried explicitly for instance in Ref. 154. Their starting point was an IBM2 Hamiltonian of the form

$$H_B = E_0 + \varepsilon_d (n_{d\pi} + n_{d\nu}) + KQ_\pi \cdot Q_\nu + \lambda M. \tag{3.43}$$

After having followed the above prescriptions, by making an expansion in θ and keeping the quadratic terms in the angular momenta $L_{k,\mu}$ they obtained, to lowest order in the $1/N$ expansion, apart from a constant

$$H = \sum_{k=\pi,\nu} \frac{1}{\Im_k} (\rho_{k2}^2 + \rho_{k2}^2) + \frac{1}{\Im_{\pi\nu}} \rho_\pi \cdot \rho_\nu + \frac{1}{2} C \theta^2, \tag{3.44}$$

where $\rho_{k\mu} = (1/N_k) L_{k\mu}$. The inertial parameters $\Im_k$ and $\Im_{\pi\nu}$ and the restoring force constant are complicated functions of N_k, β_k and of the other parameters entering into the starting Hamiltonian.

The classical Hamiltonian (3.44) is formally identical to the TRM Hamiltonian (2.3). The only difference is the presence of the coupling term $L_\pi \cdot L_\nu$, which in the TRM appears only for $N \neq Z$.

One can therefore requantize the Hamiltonian by following the TRM procedure and obtains as in the TRM a two-dimensional HO Hamiltonian in θ. The excitation energy ω of the mode is now given by

$$\omega = \frac{4}{N} \left[C \left(\frac{2}{\Im_k} - \frac{1}{\Im_{\pi\nu}} \right) \right]^{1/2}. \tag{3.45}$$

The moment of inertia and the restoring force constant are estimated using standard IBM parameters. Taking the average value $1/\Im = 1/\Im_\pi + 1/\Im_\nu$, one gets for ^{156}Gd $\omega = 2.96$ MeV which is a good approximation to the observed value $\omega = 3.1$ MeV.

We have pointed out already that the IBM and TRM form factors practically coincide up to moderate values of the momentum transfer. The IBM is more successful at higher momenta. The success of the IBM over the semiclassical description is generally attributed to the fact that in IBM the neutron-proton rotational oscillation is performed by valence nucleons only. In order to check this point it was assumed in the TRM that only the part of proton and neutron fluids external to an inert core takes part to the motion [158]. Such a change, however, spoils the agreement of the TRM with the experimental form factor. The success of the IBM description is rather to be ascribed to dynamical correlations which, among other things, allow, though effectively, for spin contributions. In particular the rather satisfactory agreement of the $M1$ IBM form factor with experiments at high q's is due to the spin degrees of freedom which are effective only at high momentum transfer.

Though accounting well for the collective properties of the $M1$ mode, the IBM2, as all other phenomenological approaches, cannot account for the $M1$ strength distribution. The attempts to explain the fragmentation of the strength by including additional bosons [25,28] or by changing the parameters of the Majorana force [159] resulted clearly inadequate.

4. MICROSCOPIC DESCRIPTIONS: SHELL-MODEL CALCULATIONS

All boson descriptions are based on the quantization of the quadrupole shape variables α_p and α_n and lead in the geometric limit to a semiclassical description formally equivalent to the one provided by the TRM.

Important differences however appear among the same boson descriptions when these are in quantized form. This is to be expected since the Hamiltonians and the methods used to handle the eigenvalue problem differ from model to model. In particular a major difference between IBM and the other two models can be noticed. While in fact the IBM is a boson number conserving scheme, the other two approaches are not.

The microscopic implications of such a difference are of great importance. The IBM bosons, as we saw, can be considered to lowest order as highly correlated valence nucleon pairs. The bosons in the NPD and the GCS models are instead to be viewed to lowest order as highly correlated p-h nucleon states. The IBM can be indeed considered as a truncated shell-model scheme where valence nucleons are so strongly pairwise correlated to allow a description in terms of bosons. The microscopic counterpart of NPD and CGSM is to lowest order the random phase approximation (RPA) scheme.

The microscopic descriptions of the scissors mode fall indeed in these too major schemes, standard shell-model and RPA. The shell model has been adopted to study $M1$ excitations only in light and medium-light nuclei. In heavy nuclei, calculations of this kind are prohibitive because of the exceedingly large dimensions of the configuration space. Only shell-model calculations using group theoretical basis and relying on severe approximations have been carried out for these latter nuclei.

A. Shell-Model Approaches in Light Nuclei. Zamick [39—41] has shown that $M1$ states with a strength of about $1\mu_N^2$ can be generated in the restricted $f_{7/2}^n$ shell-model space. These states have the form

$$\Psi_J = \sum_{L_p L_n \upsilon} D_J(L_p L_n \upsilon)[(f_{7/2}^2)_{L_p} \otimes (f_{7/2}^n)_{L_n}]^J, \tag{4.1}$$

where υ is the seniority quantum number, D_J is the probability amplitude for two protons, coupled to angular momentum L_p, and n neutrons coupled to angular momentum L_n, to couple to total spin J.

The $M1$ operator induces a transition from the $J^\pi = 0^+$ ground state to the $J^\pi = 1^+$ excited states with a strength

$$B(M1, 0^+ \to 1^+) = |\langle \Psi_{1^+} || \mathcal{M}(M1)) || \Psi_{0^+} \rangle|^2 =$$

$$= (3/4\pi)\, \mu_N^2 (g_p - g_n)^2 \left| \sum_{L\upsilon} D_0(LL\upsilon)\, D_1(LL\upsilon) \sqrt{L(L+1)} \right|^2, \qquad (4.2)$$

where the proton and neutron gyromagnetic factors are the effective ones appropriate for a single j shell

$$g = \frac{l}{j} g_l + \frac{g_s}{2j}. \qquad (4.3)$$

Using the orthogonality relation

$$\sum_\alpha D_{J\alpha}(LL)\, D_{J\alpha}(L'L') = \delta_{LL'} \qquad (4.4)$$

it is straightforward to obtain the integrated strength

$$\sum_\alpha B^\alpha(M1, 0^+ \to 1^+_\alpha) = (3/4\pi)\, \mu_N^2 (g_p - g_n)^2 \sum_L |D_0(LL)^2|^2 L(L+1). \qquad (4.5)$$

The appearance of the factor $(g_p - g_n)$ stresses the isovector character of the transitions. The scissors nature can be proved by rendering explicit the link with the TRM. Indeed

$$\sum_L |D_0(LL)|^2 L(L+1) = \langle \Psi_0 | J_p^2 | \Psi_0 \rangle =$$

$$= \frac{1}{4} \langle \Psi_0 | S^2 | \Psi_0 \rangle = \frac{1}{4} \Im\omega. \qquad (4.6)$$

We then get the standard TRM expression (2.11). In this case, however, the strength gets contribution from both the orbital and the spin components. This is due to the fact that the calculation is carried out within a single j shell so that the $M1$ operator takes the form (2.63) with effective gyromagnetic ratios (4.3). Similar expressions have been derived for the strengths of magnetic transitions of higher multipolarity ($\lambda = 3, 5, 7$).

Numerical calculations have been performed for Ti isotopes using a nucleon-nucleon interaction empirically determined from the observed levels of ^{42}Sc under the assumption that these ^{42}Sc states are due to the configuration $(1f_{7/2})^2$. The numerical results show that the $M1$ transition strength is mostly concentrated into the lowest $J^\pi = 1^+$ state. The strengths of the transitions of higher multipolarity are instead strongly fragmented and get a spin contribution

which increases with the multipolarity, a result also found by Heyde and Sau [160].

The schematic shell-model underestimates the orbital, with respect to spin, contribution to the $M1$ strength. For ^{46}Ti the calculated ratio is $R = \sqrt{B_l}/\sqrt{B_l} \simeq$ $\simeq 0.86$, while the observed one is $R \simeq 3.5$. If configuration mixing with higher shell is accounted for [161,162] the ratio raises to $R \simeq 2.5$. The calculation reproduces nicely the $M1$ and $M3$ form factors.

Studies of the $M1$ mode in Ti isotopes have been carried out with satisfactory and, in many ways, similar results also in RPA [71].

B. $SU(3)$ Shell Model. It has been pointed out already that the $M1$ mode is excited through the operator

$$S_+ = L_+^{(p)} - L_+^{(n)}. \tag{4.7}$$

If we confine ourselves within a major shell and use a HO basis, $L_+^{(\tau)}$ can be viewed as the generators of the $SU_\tau(3)$ groups. The connection with this group can be made more transparent by observing that

$$S_+ |0\rangle = -(8\pi/15)^{1/2} m(\omega_1 + \omega_3) \sum_n |K^\pi = 1^+, n\rangle \langle K^\pi = 1^+ n | Q_{+1} | 0\rangle, \tag{4.8}$$

where

$$Q = r_p^2 Y_{2,1}(r_p) - r_n^2 Y_{2,1}(r_n). \tag{4.9}$$

Namely, $L_+^{(\tau)}$ acts just like the quadrupole operators $Q_{+1}^{(\tau)}$ which are also generators of $SU_\tau(3)$.

In the $SU(3)$ model [163] the Hamiltonian is composed of an HO one-body term H_0 plus a quadrupole-quadrupole (Q-Q) two-body potential. For a given major shell this interaction represents the leading term in the expansion of any long range Wigner interaction. Its use is therefore justified in the LS coupling limit. This is the case of light nuclei. For these nuclei, isospin is also a good quantum number. The states must therefore belong to the antisymmetric representation of the group $SU(3) \otimes SU_{\sigma\tau}(4)$. Being the orbital space of a major shell of degeneracy s, the states with a given symmetry can be classified according to the irreps of the $U(s)$, $U(3)$ and $SO(3)$. If the spin-isospin components are characterized by S and T, the basis states can be written

$$|\Psi_\alpha\rangle = |[f](\lambda\mu)\, K\, L M\, S\, T\rangle, \tag{4.10}$$

where $[f]$ and $(\lambda\mu)$ label the $U(s)$ and the $U(3)$ representations, respectively, KLM are the rotational quantum numbers, while S and T label the spin and isospin wave function. The scissors states are obtained by acting with the scissors operator S_+ on the ground state. In ^{20}Ne for instance the $M1$ state is

$$|1^+T=1\rangle = S_+ |[4](80)\,K=0\,L=J=0\,S=0\,T=0\rangle = \\ = |[31](61)\,K=1\,L=1\,S=0\,T=1\rangle. \tag{4.11}$$

It is worth noticing that the generator S_+ turns the completely symmetric (antisymmetric) orbital (spin-isospin) part into one of mixed symmetry. In other nuclei with $T\neq 0$ like ^{22}Ne, S_+ generates more than one scissors state.

A shell-model $SU(3)$ study of $M1$ excitations in light nuclei of the sd shell, like ^{20}Ne, ^{22}Ne and ^{36}Ar, and of the *pf* shell, like ^{44}Ti, was carried out by Poves et al. [45—47]. The findings of their calculation were:

i) The integrated $M1$ strength of all $J^\pi = 1^+$ states is $\sum B(M1) = 2.43\,\mu_N^2$ in ^{20}Ne and $\sum B(M1) = 3.60\,\mu_N^2$ in ^{36}Ar.

ii) In ^{20}Ne the 75% of the strength is concentrated into the lowest $J^\pi = 1^+$ state at $\omega \simeq 11$ MeV and mostly comes from the convection current.

iii) In ^{36}Ar the strength is mainly shared by four $J^\pi = 1^+$ states. The difference between the $M1$ distribution in the well deformed ^{20}Ne and that in the vibrational ^{36}Ar can be interpreted as a confirm of the peculiarity of the scissors mode, whose existence is closely related to deformation according to the TRM and the schematic RPA.

In heavy nuclei the $SU(3)$ symmetry is spoiled by the strong spin-orbit coupling term. This causes a large separation between the members of the Nilsson spin-orbit doublets and pushes the state of maximum j down to the next lower major shell. As a result a major shell is composed of a set of normal parity orbits and one abnormal parity s.p. state.

One can observe, however, that the states of a given N shell with $l-1/2$ and $(l-2)+1/2$ are very close in energy [164—166]. Exploiting the fact that the normal parity states of a given shell have the same total angular momenta as the levels of an oscillator shell with $N=N-1$, one can make the mapping $N\to N-1$, $l-1/2\to l+1/2=(l-1)+1/2$, $(l-2)+1/2\to(l-1)-1/2$.

After relabeling the Nilsson states with pseudo-oscillator quantum numbers $[\tilde{N}\tilde{n}\tilde{\Lambda}\tilde{\Omega}]$, the members of the new spin-orbit doublet with $\tilde{\Omega}=\tilde{\Lambda}\pm 1/2$ appear very close in energy. The normal parity states can therefore be classified according to a pseudo-$SU(3)$ [167,168]. Such a scheme can work only under the assumption that i) particles in the abnormal parity single j shell are dominated

by the pairing interaction so that the dominant configurations arising from this shell are zero seniority states with $J^A_\pi = J^A_\nu = 0$, ii) the interaction between normal and abnormal parity states is weak, iii) proton and neutron spatial wave functions in the normal parity space are totally symmetrical so that $\tilde{S}_\pi = \tilde{S}_\nu = 0$. Under these assumptions, the nuclear state is of the form [48,49]

$$\Psi_{JM} = (\Psi^N_{JM} \otimes \Psi^A_{JA})_{JM}, \tag{4.12}$$

where the completely antisymmetric normal parity (Ψ^N_{JM}) and abnormal parity (Ψ^A_{JA}) states are respectively classified according to the chains

$$U(\Omega^\sigma_N) \to U(\Omega_{N/2}) \otimes U(2) \to SU(3) \otimes SU(2) \to O(3) \otimes SU(2) \to SU(2)$$

$$U(\Omega^\sigma_A) \to S_p(\Omega^\sigma_A) \to O(3), \tag{4.13}$$

where Ω_N and Ω_A are the dimensions of the two groups and S_p is the compact symplectic group. Because of the pseudospin s.p. basis and the assumptions made, the magnetic dipole operator $\mathcal{M}(M1)$ is purely orbital

$$\mathcal{M}(M1) = 1/2(g_\pi + g_\nu)\tilde{L} + 1/2(g_\pi - g_\nu)(\tilde{L}_\pi - \tilde{L}_\nu). \tag{4.14}$$

The theory predicts from one to four $J^\pi = 1^+$ states, the actual number depending on the leading $SU(3)$ proton and neutron irreps. For completely symmetric proton and neutron $SU(3)$ representations $(\lambda_\pi, 0)(\lambda_\nu, 0)$, as in ^{154}Sm and ^{238}U, there is only one $J^\pi = 1^+$ state. For such a state the $M1$ transition strength is given by

$$B(M1, J^\pi = 0 \to 1^+) = 364\pi(g_\pi - g_\nu)^2 \frac{2\lambda_\pi \lambda_\nu}{(\lambda_\pi + \lambda_\nu - 1)} \tag{4.15}$$

which has the same structure as in IBM2 expression (eq. 3.29), with λ_τ replacing N_τ.

When only one π (or ν) irreps is symmetric, as in ^{156}Gd, there are two $J^\pi = 1^+$ states, both collective. In general, as in ^{164}Dy or ^{168}Er, neither the $SU_\pi(3)$ nor the $SU_\nu(3)$ irreps are symmetric. In this case there are four $J^\pi = 1^+$ states, three of them corresponding to $K^\pi = 1^+$ bands and the other belonging to a $K^\pi = 0^+$ band. Only two of the three $J^\pi = 1^+$ states have large $M1$ strength, while the state belonging to the $K^\pi = 0^+$ band is moderately collective.

Aside from the $M1$ strengths, the authors have calculated also the magnetic moments μ, which fixed the gyromagnetic factors ($g_\pi = 1$ and $g_\nu = 0$), as well as the branching ratio $B(M1, 1^+ \to 2^+)/B(M1, 1^+ \to 0^+)$ which supports the axial symmetry of the nuclei under study. The calculations underestimate the $M1$ strength by about a factor two.

5. RPA DESCRIPTIONS

Most of the experimental analyses have been devoted to the search for and characterization of the mode in heavy nuclei, specially of the rare-earth region. A main feature of the mode in these nuclei is the fragmentation of the $M1$ strength. None of the phenomenological or schematic approaches discussed previously can account for such a property. Full shell-model studies would be needed. They are not feasible, however, for heavy nuclei. One must therefore rely on approximations. RPA has been the approximation scheme more extensively adopted.

A. RPA General Formalism. In RPA the nuclear eigenvalue problem is formally turned into a HO eigenvalue equation [169,170]. To this purpose one defines the eigenstates of the nuclear Hamiltonian as

$$|\lambda\rangle = O_\lambda^+ |0\rangle, \tag{5.1}$$

where the operators O_λ^+ are such that its hermitian conjugates satisfy the equation

$$O_\lambda |0\rangle = 0. \tag{5.2}$$

The latter equation defines the nuclear ground state $|0\rangle$ as the vacuum for the operators O_λ and O_λ^+. Such a vacuum is in general a highly correlated state. Because of the above assumptions the eigenvalue equation can be written in the HO form

$$[H, O_\lambda^+] |0\rangle = \omega_\lambda O_\lambda^+ |0\rangle = (E_\lambda - E_0) O_\lambda^+ |0\rangle. \tag{5.3}$$

RPA consists in solving these equations in a restricted p-h space so that the operator O_λ^+ is of the form

$$O_\lambda^+ = \sum (Y_{ph}^\lambda a_p^+ a_h - Z_{ph}^\lambda a_h^+ a_p). \tag{5.4}$$

The states $|\lambda\rangle$ are normalized according to

$$\delta_{\lambda\lambda'} = \langle\lambda|\lambda'\rangle = \langle 0|O_\lambda O_{\lambda'}^+|0\rangle = \langle 0|[O_\lambda, O_{\lambda'}^+]|0\rangle \cong \langle|[O_\lambda, O_{\lambda'}^+]|\rangle, \qquad (5.5)$$

where $|\rangle$ is the p-h vacuum. The last approximate equality expresses the quasi-boson approximation. In virtue of this approximation, the normalization condition yields

$$\sum_{ph} (Y_{ph}^{\lambda *} Y_{ph}^{\lambda'} - Z_{ph}^{\lambda *} Z_{ph}^{\lambda'}) = \delta_{\lambda\lambda'}. \qquad (5.6)$$

The RPA eigenvalue equations are

$$\begin{vmatrix} A & B \\ B^* & A^* \end{vmatrix} \begin{vmatrix} Y_\lambda \\ Z_\lambda \end{vmatrix} = \hbar\omega_\lambda \begin{vmatrix} Y_\lambda \\ -Z_\lambda \end{vmatrix} \qquad (5.7)$$

where

$$A_{ph,\,p'h'} = \langle|[a_h^\dagger a_p, [H, a_{p'}^\dagger a_{h'}]]|\rangle = (\varepsilon_p - \varepsilon_h)\,\delta_{pp'}\delta_{hh'} + V_{ph'h'p},$$

$$B_{ph,\,p'h'} = -\langle|[a_p^\dagger a_h, [H, a_{h'}^\dagger a_{p'}]]|\rangle = V_{pp'hh'}. \qquad (5.8)$$

The transition amplitudes for the generic one-body operator W are given by

$$\langle\lambda|W|0\rangle = \langle 0|[O_\lambda, W]|0\rangle \cong \langle|[O_\lambda, W]|\rangle =$$

$$= \sum_{ph} (Y_{ph}^{\lambda *} W_{ph} + Z_{ph}^{\lambda *} W_{hp}). \qquad (5.9)$$

In QRPA the states have the form

$$|\lambda\rangle = O_\lambda^\dagger|0\rangle = \sum \{Y_{\alpha\beta}^\lambda \alpha_\alpha^\dagger \alpha_\beta^\dagger - Z_{\alpha\beta}^\lambda \alpha_\beta \alpha_\alpha\}|0\rangle, \qquad (5.10)$$

where $\alpha_\alpha^\dagger(\alpha_\alpha)$ are creation (destruction) quasiparticle operators defined by the Bogoliubov transformation

$$\alpha_\alpha^\dagger = u_\alpha a_\alpha^\dagger - \upsilon_\alpha a_\alpha, \qquad u_\alpha^2 + \upsilon_\alpha^2 = 1. \qquad (5.11)$$

The QRPA eigenvalues are obtained by still solving eqs.(5.7) with matrix elements

$$A_{\alpha\beta,\,\gamma\delta} = \langle 0|[\alpha_\beta\alpha_\alpha, [H, \alpha_\gamma^\dagger\alpha_\delta^\dagger]]|0\rangle \cong (E_\alpha + E_\beta)\,\delta_{\alpha\gamma}\delta_{\beta\delta} + \tilde{V}_{\alpha\beta\gamma\delta},$$

$$B_{\alpha\beta,\,\gamma\delta} \simeq \langle 0|[\alpha_\beta\alpha_\alpha, [H, \alpha_\delta\alpha_\gamma]]|0\rangle \cong \tilde{V}'_{\alpha\beta\gamma\delta}\ , \qquad (5.12)$$

where E_α is the quasiparticle energy and $|0\rangle$ is now the quasiparticle vacuum. We omit the explicit expressions of $\tilde{V}_{\alpha\beta\gamma\delta}$ and $\tilde{V}'_{\alpha\beta\gamma\delta}$ which are rather involved and can be found for instance in Ref.169.

The QRPA transition amplitudes for the generic operator W are given by

$$\langle \lambda | W | 0 \rangle \simeq \langle 0 | [O_\lambda, W] | 0 \rangle =$$

$$= \sum_{\alpha > \beta} (Y^{\lambda *}_{\alpha\beta} W_{\alpha\beta} + Z^{\lambda *}_{\alpha\beta} W_{\beta\alpha}) (u_\alpha v_\beta + \tau v_\alpha u_\beta), \tag{5.13}$$

where $\tau = +1$ or -1 according that the operator W is even or odd under time-reversal.

The eigenvalues and the transition amplitudes can be determined only numerically using a proper s.p. deformed basis. In the BCS approach only the coefficients u_α and v_α are determined selfconsistently using the pairing force only, while the s.p. basis is determined independently. In Hartree–Bogoliubov (H.B.) both s.p. states u_α and v_α and coefficients are to be determined self-consistently from a unique interaction.

B. RPA Hamiltonians. The first studies of the mode have been carried out in schematic RPA [34—37]. As already pointed out, their results coincide with those derived in Sec.IID for the TRM. We therefore will not report on them. We only like to mention that a schematic calculation which accounts also for spin-admixtures was carried out to compute the $M3$ transition [171]. The results were close to the ones derived for the TRM [106].

Apart from few calculations using a Skyrme interaction [55] or a Landau–Migdal force [59,67,68], most of the realistic studies have been carried out using a separable interaction either in RPA [52—54,56—58,60—66,69—77] or in Tamm–Dancoff approximation [78,79].

A guide for guessing which multipoles should enter in the interaction is provided by phenomenological and schematic models. From their analysis we can infer that an RPA Hamiltonian should contain at least the following terms

$$H = H_0 + V_{P-P} + V_{Q-Q} + V_{\sigma\sigma}. \tag{5.14}$$

The first term is a one-body deformed Hamiltonian

$$H_0 = \sum_i h_i = \sum_i (T_i + V_i), \tag{5.15}$$

where T_i is the nucleon kinetic term; and V_i, the nucleon deformed potential. This is either of the Nilsson [78] or Woods–Saxon form (for instance [53,60]). The p-h energy spectrum produced by the one-body potential is extremely fragmented with intermixed orbital and spin excitations [172,173].

The second piece is the monopole and quadrupole pairing for protons and neutrons

$$V_{P-P} = \sum_{k=p,n} \{G_0^{(k)} P_0^{(k)\dagger} P_0^{(k)} + G_2^k P_2^{(k)\dagger} P_2^{(k)}\}, \tag{5.16}$$

where

$$P_J^\dagger = \sum_{\alpha,\beta} [a_\alpha^\dagger \otimes a_\beta^\dagger]_J. \tag{5.17}$$

The third is the Q–Q interaction which in the isospin formalism is

$$V_{Q-Q} = 1/2 \sum_{T=0,1} \chi_Q(T)\, [Q(T)\, Q^\dagger(T) + Q^\dagger(T)\, Q(T)], \tag{5.18}$$

where

$$Q\left(T = \begin{matrix} 0 \\ 1 \end{matrix}\right) = Q_{+1}^{(p)} \pm Q_{+1}^{(n)}. \tag{5.19}$$

Finally we have the spin-spin interaction

$$V_{\sigma\sigma} = 1/2 \sum_{T=0,1} \chi_\sigma(T)\, [\sigma(T)\, \sigma^\dagger(T) + \sigma^\dagger(T)\, \sigma(T)], \tag{5.20}$$

where

$$\sigma\left(T = \begin{matrix} 0 \\ 1 \end{matrix}\right) = s_{+1}^{(p)} \pm s_{+1}^{(n)}. \tag{5.21}$$

The importance of the Q–Q and monopole pairing interactions appears clear from the microscopic analysis of the TRM or, which amounts to the same thing, from schematic RPA calculations (Sec. 2D). As shown there, the quadrupole fields are related closely to proton and neutron angular momenta. They enter directly in the $M1$ p-h channel. Monopole pairing qualifies the rotors as superfluids and has the effect of quenching the $M1$ strength without spoiling the scissors picture. The necessity of the quadrupole pairing can be inferred from the fact that the $L = 2$ correlated valence pairs are the building blocks of the IBM states. The major role played by such a term emerges explicitly from displaying the structure of the schematic SM wave function [39]

$$\Psi_0 = D_0(L_p = 0, L_n = 0)\,|0\rangle + D_0(L_p = 2, L_n = 2)\,|(2_p \otimes 2n)_0\rangle,$$

$$\Psi_1 = D_1(L_p = 2, L_n = 2)\,|(2_p \otimes 2_n)_1\rangle. \tag{5.22}$$

The $M1$ transition is clearly due to the $L = 2$ correlations among alike valence nucleons. Monopole and quadrupole pairings have the effect of redistributing the p-h $M1$ spectrum by inducing a concentration of scissors excitation around

3 MeV [172,173]. The role of quadrupole pairing in RPA was studied in Ref.70. The spin-spin term is dictated by the spin-orbit admixtures in the s.p. states and by a large number of low energy p-h spin excitations intermixed with the orbital ones. Because of its repulsive character, the spin-spin interaction has the important effect of pushing up in energy the spin excitations, which get separated from the $M1$ orbital transitions, consistently with experiments and with the scissors picture [78].

Although all terms included in eq.(5.14) play a major role, it is not excluded that other pieces of the nuclear Hamiltonian not present in eq.(5.14) may affect the $M1$ channel. It has been stressed for instance that the so-called recoil term reduces the fragmentation of the two-quasiparticle spectrum, thereby concentrating the strength around a main peak consistently with experiments, and enforces the scissors nature of the transitions [174—176].

C. Spurious Rotational Admixtures. The study of the mode in a realistic RPA approach has gone through a series of problems [177]. A major one was the occurrence of spurious rotational admixtures pointed out for the first time in Ref.60. Since the RPA eigenvalue problem is formulated in the intrinsic system, the RPA ground state breaks spherical symmetry so that

$$J_{+1}|0\rangle \neq 0. \tag{5.23}$$

This state separates out at zero energy from the other RPA states if the starting Hamiltonian is rotationally invariant. In this case in fact we have

$$(H - E_0)\, J_{+1}|0\rangle = [H, J_{+1}]|0\rangle = 0. \tag{5.24}$$

Namely, $J_{+1}|\rangle$ is an exact eigenstate with zero eigenvalue. It is therefore automatically orthogonal to the other RPA states.

The Hamiltonian used in almost all calculations however is not rotationally invariant so that

$$\langle K^\pi = 1^+|J_{+1}|0\rangle \neq 0. \tag{5.25}$$

Several techniques have been developed to remove the rotational state. The first one [60] consists in adding a symmetry restoring term to the Hamiltonian

$$H \to H' = H - \sum \nu\lambda_\nu J_- O_\nu^+(K^\pi = 1^+), \tag{5.26}$$

where the Lagrange multipliers λ_ν are determined by the constraint

$$\langle K^\pi = 1^+, \nu|J_+|0\rangle = \langle 0|O_\nu(K^\pi = 1^+)\, J_+|0\rangle = 0. \tag{5.27}$$

Since such a condition depends upon the solution, the RPA equations become nonlinear, so that their final determination requires an iterative procedure.

A second procedure, adopted in TDA [78], consists in using the Schmidt orthogonalization procedure on the two-quasiparticle states. These have the form

$$|\alpha_1\alpha_2\rangle = |\alpha_1\alpha_2\rangle_{sp} - J_+ |0\rangle \langle 0| J_- |\alpha_1\alpha_2\rangle_{sp}. \tag{5.28}$$

The states so constructed are no longer eigenstates of the starting unperturbed Hamiltonian, so that an iterative procedure is needed also in this case.

A third one, adopted in Ref.72, consists in using Pyatov prescription [178] of replacing the quadrupole field in the Hamiltonian with

$$F_1^{(\tau)} = [H_0, J_+^{(\tau)}]. \tag{5.29}$$

The condition of rotational invariance

$$[H, J_+] = 0 \tag{5.30}$$

imposes on the fields F the following constraint

$$\begin{aligned} 1 + k_{pp} \langle [F_1^{(p)\dagger}, J_+^{(p)}] \rangle + k_{nn} \langle [F_1^{(n)\dagger}, J_+^{(n)}] \rangle = 0, \\ 1 + k_{nn} \langle [F_1^{(n)\dagger}, J_+^{(n)}] \rangle + k_{pp} \langle [F_1^{(p)\dagger}, J_+^{(p)}] \rangle = 0. \end{aligned} \tag{5.31}$$

In other approaches [77] the problem is avoided by using a j-projected s.p. basis which enables one to formulate the problem directly in the laboratory frame. Finally the separation can be achieved by using a selfconsistent basis. This has been done in Ref.61 and partly in Ref.55. The problem can be clearly illustrated in schematic RPA [179].

D. Selfconsistent Fields and Rotational Admixtures: A Simple Approach. Let us assume [179] that Z protons and N neutrons move in a spherical HO mean field with frequency ω_0 and interact through a $Q - Q$ force. The Hamiltonian is therefore of the rotational invariant form

$$\begin{aligned} H = H_0 + \frac{1}{2} \chi \sum_{\mu} (Q_{2\mu}^{(p)*} Q_{2\mu}^{(p)} + Q_{2\mu}^{(n)*} Q_{2\mu}^{(n)}) + \\ + \frac{1}{2} \chi_{pn} \sum_{\mu} (Q_{2\mu}^{(p)*} Q_{2\mu}^{(n)} + Q_{2\mu}^{(n)*} Q_{2\mu}^{(p)}), \end{aligned} \tag{5.32}$$

where

$$Q_{2\mu}^{(\tau)} = \sum_i q_{2\mu}^{(\tau)}(i) = \sum_i r_i^{(\tau)} Y_{2\mu}^{(\tau)}(i). \tag{5.33}$$

1. Selfconsistent Mean Field and Doubly-Stretched Coordinates. In the Hartree approximation we obtain for the i_{th} proton or neutron deformed mean field

$$V_H^{(\tau)} = \frac{1}{2} m\omega_0^2 r^2 - \beta_\tau m\omega_0^2 q_{20}^{(\tau)}, \tag{5.34}$$

having defined

$$\chi \langle Q_{20}^{(p)} \rangle + \chi_{pn} \langle Q_{20}^{(n)} \rangle = -\beta_p m\omega_0^2,$$

$$\chi \langle Q_{20}^{(n)} \rangle + \chi_{pn} \langle Q_{20}^{(p)} \rangle = -\beta_n m\omega_0^2. \tag{5.35}$$

The Hartree potential can be written in the form of an anisotropic HO potential

$$V^{(\tau)} = \frac{1}{2} m\omega_1^2(\tau) \left(x_1^{(\tau)^2} + x_2^{(\tau)^2}\right) + \frac{1}{2} m\omega_3^2(\tau) x_3^{(\tau)^2} \tag{5.36}$$

with frequencies

$$\omega_1(\tau) = \omega_0 \sqrt{1 + \frac{2}{3}\delta_\tau} \simeq \omega_0 \left(1 + \frac{1}{3}\delta_\tau\right),$$

$$\omega_3(\tau) = \omega_0 \sqrt{1 - \frac{4}{3}\delta_\tau} \simeq \omega_0 \left(1 - \frac{2}{3}\delta_\tau\right), \tag{5.37}$$

where $\delta_\tau = \sqrt{45/(16\pi)}\,\beta_\tau$. The same potential can be put in the «spherical» form

$$V^{(\tau)} = \frac{1}{2} m\omega_0^2 (\tilde{x}_1^{(\tau)^2} + \tilde{x}_2^{(\tau)^2} + \tilde{x}_3^{(\tau)^2}) \tag{5.38}$$

if we use double stretched coordinates [180—183] $\tilde{x}_i = \omega_i/\omega_0 x_i$. These are to be used in the quadrupole operator entering into the $Q - Q$ Hamiltonian so as to preserve its spherical character. This transformation indeed ensures that the Hartree field is not further distorted once the interaction is switched on. We have in fact

$$\langle \tilde{Q}_{20}^{(p)} \rangle = \langle \tilde{Q}_{20}^{(n)} \rangle = 0 \tag{5.39}$$

if we impose the conditions

$$\omega_1^{(\tau)} \sum_1^\tau = \omega_2^{(\tau)} \sum_2^\tau = \omega_3^{(\tau)} \sum_3^\tau, \tag{5.40}$$

where $\sum_i^\tau = \sum_i (n_i + 1/2)$. The explicit form of the $\tilde{Q}$ operators is

$$\tilde{Q}_{\pm 1} = \frac{\omega_1 \omega_3}{\omega_0^2} Q_{\pm 1}, \qquad \tilde{Q}_{\pm 2} = \frac{\omega_1^2}{\omega_0^2} Q_{\pm 2},$$

$$\tilde{Q}_0 = \frac{1}{3\omega_0^2} (\omega_1^2 + 2\omega_3^2) Q_0 - \frac{\sqrt{5}}{3\omega_0^2} (\omega_1^2 - \omega_3^2) r^2 Y_{00}. \tag{5.41}$$

Since the double stretched quadrupole operator contains also a monopole term, the new Q–Q potential is composed of pure quadrupole-quadrupole plus monopole-quadrupole and monopole-monopole terms.

The Hartree conditions fix the isoscalar coupling constant. Summing the two eqs.(5.34) and making use of standard formulas for the quadrupole moments, we obtain, to lowest order in δ, the well-known result [133]

$$\chi(0) = \frac{1}{2} (\chi + \chi_{pn}) \simeq - \frac{4\pi}{5} \frac{m\omega_0^2}{A\langle r^2 \rangle}. \tag{5.42}$$

The isovector coupling constant $\chi(1)$ can be derived from the symmetry energy mass formula [133] and results to be related to $\chi(0)$ by the ratio $b = -\chi(1)/\chi(0) \simeq 3.6$. According to some analyses [75,184], however, this value is too large.

A quasiparticle RPA calculation formulated in the $\Delta N = 0 + 2$ space has been carried out [179]. It is shown that, in virtue of the selfconsistent conditions (5.35), the schematic quasiparticle RPA gives a vanishing root. This is the eigenvalue of the redundant rotational mode. Such a state results to be completely removed from the intrinsic ones. One obtains indeed

$$\langle n, K^\pi = 1^+ | L_+ | 0 \rangle \propto P(x) = x^3 + ax^2 + bx + c = 0, \tag{5.43}$$

where $P(x) = P(\omega^2) = 0$ is the eigenvalue equation giving the roots of the $M1$ physical states.

The method presented here to remove the spurious rotational state, though developed within schematic RPA, has a more general valence. Indeed, the Hartree conditions (5.35) can be written in the form

$$1 + k_{pp} \langle [F_1^{(p)\dagger}, J_+^{(p)}] \rangle + k_{pn} \langle [F_1^{(n)\dagger}, J_+^{(n)}] \rangle = 0,$$

$$1 + k_{nn} \langle [F_1^{(n)\dagger}, J_+^{(n)}] \rangle + k_{pn} \langle [F_1^{(p)\dagger}, J_+^{(p)}] \rangle = 0, \tag{5.44}$$

where

$$F_1^{(\tau)} = [H_0, J_+^{(\tau)}]. \tag{5.45}$$

These are just Pyatov ansatz (5.31) for removing the rotational mode. They are therefore valid for any one-body potential and any separable Hamiltonian.

2. Scissors Sum Rule in RPA. It has been pointed out already that for the scissors mode the energy weighted $M1$ sum rule is given by eq.(2.66). This quantity has been computed in phenomenological domains such as IBM2 [79, 86—88], in spherical shell-model [42] and in a schematic approach using a deformed mean field (no interaction) [81]. Recently the same sum rule has been computed in RPA [185]. To this purpose a separable interaction which includes a Q–Q interaction with double stretched coordinates has been adopted. The final result was

$$S_{EW}^{(sc)}(M1) = \frac{3}{16\pi}(S_1^{(sc)} + S_{20}^{(sc)} + S_{22}^{(sc)})\, g_r^2\, \mu_N^2. \tag{5.46}$$

The first term comes from the Hartree field and is given by

$$S_1^{(sc)} = \frac{1}{2}\sum_{\mu=\pm 1} \langle 0 \,|\, [S_\mu^\dagger, [H_0, S_\mu]] \,|\, 0\rangle =$$

$$= 3m\omega_0^2(\beta_p \langle Q_{20}^{(p)}\rangle + \beta_n \langle Q_{20}^{(n)}\rangle) \tag{5.47}$$

which is what obtained in Ref. 81, where only a deformed mean field is considered. The second piece comes from the two-body interaction involving the monopole operators and is given by

$$S_2^{(0)} = -3m\omega_0^2(\beta_p \langle Q_{20}^{(p)}\rangle + \beta_n \langle Q_{20}^{(n)}\rangle). \tag{5.48}$$

It is, namely, equal and opposite to the one-body contribution (5.47), which therefore cancels out. It remains therefore only the contribution from the pure Q–Q potential, apart from modifications induced by the use of stretched coordinates. This is given to lowest order in δ by

$$S_{EW}^{(sc)}(M1) \simeq -\frac{9}{4\pi}\chi_{pn}\left(\sum_n B_n^{(0)}(E2)\uparrow - \sum_n B_n^{(1)}(E2)\uparrow\right) \tag{5.49}$$

which is the result obtained in spherical shell model [42]. Stretched coordinates are responsible for higher order terms which however are not negligible [185]. Experimentally the $E2$ strength to the lowest 2^+ state is by orders of magnitude larger than the strengths of the other transitions. If these are ignored, one gets

$$\omega^{(-)}B(M1)^{(-)} + \omega^{(+)}B(M1)^{(+)} \simeq -\frac{9}{4\pi}\chi_{pn}\, B_0^{(0)}(E2)\uparrow. \tag{5.50}$$

It follows that

$$B(M1)^{(\pm)} \propto B_0^{(0)}(E2)\uparrow \propto \delta^2. \tag{5.51}$$

The sum rule approach presented here gives a quite general theoretical proof of the quadratic deformation law holding for the $M1$ strengths of both low-lying and high energy scissors modes.

E. Realistic RPA Calculations. The earlier RPA calculations produced contradictory results. Some of them had seriously questioned the scissors nature of the mode [53,54,59]. The reason of these discordances can be easily explained. The $M1$ channel is extremely sensitive to s.p. energies, to the kind of interaction used and, for a given interaction, to the choice of the strengths of the different separable pieces. As already pointed [177], these early approaches used different and incomplete Hamiltonians and relied on several untested approximations. Moreover, the $M1$ states produced by these calculations were contaminated with spurious rotational admixtures. Most of the recent studies are free of most of these limitations and, consequently, tend to converge to similar results.

The goal of RPA calculations can be summarized in the following points. They should i) account for the collective properties of the mode such as the quadratic deformation dependence of the total $M1$ strength, ii) put on display the microscopic structure of the $M1$ states so as to enable one to decide about the scissors nature of the mode, iii) reproduce closely the energy distribution of the $M1$ strength.

Concerning the first point, calculations carried out by different groups have reproduced fairly well the deformation law [69,74,77,79]. The crucial role of pairing correlation in enforcing such a law was particularly stressed. As clearly illustrated in Fig.3, the agreement with experiments would be almost perfect if the spin contribution could be suppressed [74,79]. Indeed, such a good agreement is reached in Ref.77, where the spin contribution is effectively suppressed by the j-projected basis. In this basis, in fact, deformation is accounted for only perturbatively. The necessity of spin suppression dictated by the experimental data supports implicitly the scissors picture. Such a picture is tested more explicitly by computing the summed overlap

$$\sum_n |\langle K^+, n | \psi_{sc} \rangle|^2, \tag{5.52}$$

where $|\psi_{sc}\rangle$ is the scissors state defined as

$$|\psi_{sc}\rangle = \alpha J_+^{(p)} |0\rangle + \beta J_+^n |0\rangle. \tag{5.53}$$

The coefficients are determined by imposing its normalization to unit and its orthogonalization to the rotational state

$$\langle \psi_{sc} | \psi_{sc} \rangle = 1, \qquad \langle \psi_{sc} | J_+ | 0 \rangle = 0. \tag{5.54}$$

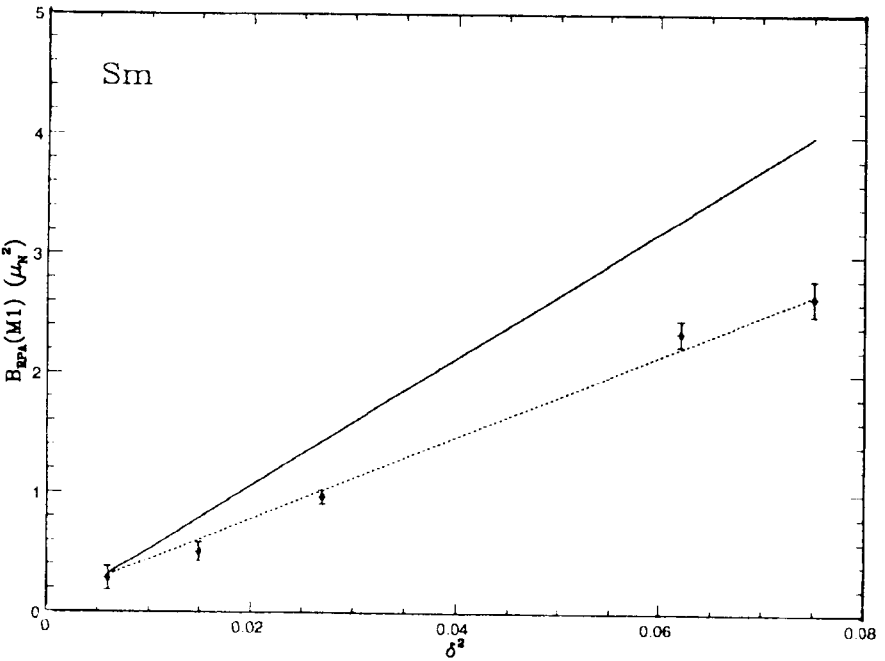

Fig.3. Deformation dependence of the $M1$ strength computed in RPA versus experiments. The dotted line gives the orbital contribution

The summed overlap for the states below 4 MeV is found to be about 40%, a very large number in view of the fact that, as discussed in Sec.2D, the model predicts another scissors state at high energy [177]. This latter mode is predicted also by realistic RPA calculations [59,68,72,76]. Its extent of fragmentation however is not settled. It seems [186] that if the two-quasiparticle space is truncated up to 30 MeV, the mode is basically not fragmented in agreement with the schematic picture [177]. It becomes strongly fragmented if the two-quasiparticle space is enlarged.

As we said, the experimental systematic study of the scissors mode has led to the other interesting discovery of spin excitations [21,22]. These have been detected in ^{154}Sm and ^{156}Gd in the energy range $5 \div 11$ MeV and have a very peculiar property. The profile of the spectrum exhibits two distinct bumps. These transitions have been studied with good success in TDA [187,188] as well as in RPA [67,68,70,74,77]. There is however no conclusive answer to the interpretation of the observed two-peak structure. It is indeed not clear whether

the two peaks correspond to different proton and neutron excitations [70,77, 187,188] or are of isovector and isoscalar nature [74]. The calculations which support the first picture use a vanishing coupling constant for the isovector spin-spin interaction. The supporters of the other interpretation use a nonvanishing value. In the first case, deformation plays an important role, in the second case, it is not relevant. This fact suggests that the issue can be settled by a systematic analysis which covers both spherical and deformed nuclei.

RPA calculations have been carried out to describe the $M1$ excitations not only in rare-earth nuclei, but also in actinides [66,73], in medium-light [71] and medium nuclei [63]. On the whole, the results are satisfactory. An unsolved problem remains however. The energy distribution of the $M1$ strength is not well reproduced. This suggests that maybe the RPA space should be enlarged so as to allow for higher configurations.

6. BEYOND RPA: THE QPNM APPROACH

Notably, TDA and RPA calculations are carried out in a p-h or two-quasiparticle space. On energetic ground, however, higher order configurations can also contribute to the mode. Many four-quasiparticle excitations fall within or just above the energy range where the low-lying $M1$ transitions are observed. In order to study the effect of these states it is necessary to enlarge the space. This has been achieved within the QPNM [93]. In this approach [94] the nuclear system is studied in a space spanned by one plus two RPA phonon states. Most of the properties of all nonrotational states up to 2.5 MeV in deformed nuclei, including all $E\lambda$ and $M\lambda$ transitions, have been studied in this scheme [189—196].

A. Brief Description of the QPNM. The starting QPNM Hamiltonian has the following structure

$$H = H_{\text{s.p.}} + H_{\text{pair}} + H_M + H_S + H_T. \tag{6.1}$$

The first term is the one-body Hamiltonian which includes a deformed axially symmetric Saxon–Wood potential, the second is a proton (neutron) monopole pairing interaction, the other three are isoscalar and isovector spin-independent (H_M), spin-dependent (H_S) and tensor (H_T) two-body interactions. All these pieces are written in separable form. The two-body interaction acts in the p-h as well as in the particle-particle (p-p) channels. The p-p component of the spin-independent part yields also a quadrupole pairing term which adds to the monopole pairing interaction. One may notice that the QPNM Hamiltonian is considerably more complex than those adopted in RPA.

The first step of the QPNM is to make use of the Bogoliubov canonical transformation and express the Hamiltonian in terms of quasiparticle operators $\alpha_{q\sigma}$ and $\alpha^{\dagger}_{q\sigma}$. The symbols $q\sigma$ stand for the s.p. asymptotic quantum numbers $q\sigma = Nn_z\Lambda\uparrow$ for $K = \Lambda + 1/2$ and $q\sigma = Nn_z\Lambda\downarrow$ for $K = \Lambda - 1/2$. RPA phonons are then constructed

$$Q^{\dagger}_{Kn\sigma} = \frac{1}{2}\sum_{q_1q_2}\{\psi^{Kn}_{q_1q_2}A^{\dagger}_{K\sigma}(q_1q_2) - \varphi^{Kn}_{q_1q_2}A_{K-\sigma}(q_1q_2)\}, \tag{6.2}$$

where $A^{\dagger}_{K\sigma}(q_1q_2)$ $(A_{K\sigma}(q_1q_2))$ are pairs of creation (annihilation) quasiparticle operators. Their actual structure can be found in Ref.194. Using the equations defining $Q^{\dagger}_{Kn\sigma}$ and $Q_{Kn\sigma}$ it is possible to bring the Hamiltonian (6.1) into the quasiparticle phonon form

$$H_{\mathrm{QPNM}} = H_q + H_{\upsilon} + H_{\upsilon q}, \tag{6.3}$$

where H_q and H_q are respectively the one-body quasiparticle and RPA phonon Hamiltonians and $H_{\upsilon q}$ is the quasiparticle phonon coupling term. Their expressions can be found in Ref.194.

The transformed Hamiltonian is finally put in diagonal form by using the variational principle with a trial wave function

$$\Psi_n(\sigma K^{\pi} = 1^+) = \{\beta\sum_i R^n_i Q^{\dagger}_{\nu} + \frac{1}{2}\sum_{\nu_1\sigma_1\nu_2\sigma_2} s^{\sigma}_{\nu_1\sigma_1\nu_2\sigma_2}P^n_{\nu_1\nu_2}Q^{\dagger}_{\nu_1\sigma_1}Q^{\dagger}_{\nu_2\sigma_2}\}\Psi_0, \tag{6.4}$$

where

$$s^{\sigma}_{\nu_1\sigma_1\nu_2\sigma_2} = \delta_{\sigma_1\mu_1+\sigma_2\mu_2,\,\sigma K}(1+\delta_{\nu_1,\nu_2})^{1/2}. \tag{6.5}$$

The labels ν and ν_k stand for the multipolarities of the RPA phonons, $\nu = (\lambda_0\mu_0)_i = (21)_i$ and $\nu_k = (\lambda\mu)_k$. The eigenvalues E_n are the roots of the secular equation

$$\det\Big\| (\omega_{\nu} - E_n)\delta_{i,i'} - \sum_{\nu_1\geq\nu_2}\frac{C(\nu_1\nu_2)\,U^{\nu}_{\nu_1\nu_2}\,U^{\nu'}_{\nu_1\nu_2}}{\omega_{\nu_1}+\omega_{\nu_2}+\Delta\omega(\nu_1\nu_2)+\Delta(\nu_1\nu_2)-E_n}\Big\| = 0, \tag{6.6}$$

where

$$C(\nu_1\nu_2) = \frac{1+K(\nu_1,\nu_2)}{1+\delta_{\nu_1,\nu_2}}. \tag{6.7}$$

The quantity ω_ν denotes the RPA energies, $U^{\nu}_{\nu_1\nu_2}$ describes the coupling between one- and two-phonon states, K is a term introduced to take into full account the Pauli principle in the two-phonon components of the total wave function (eq.(6.4)). This term induces the energy shift $\Delta\omega(\nu_1\nu_2)$ in the eigenvalue equation. The other energy shift $\Delta(\nu_1\nu_2)$ is due to the coupling with three-phonon states not included explicitly into the calculation. Its value is approximately $\Delta(\nu_1\nu_2) \simeq -0.2\Delta\omega(\nu_1\nu_2)$.

B. Calculations and Results. Numerical calculations have been carried out for a chain of Gd and Dy isotopes. Single particle energies and wave functions were computed from the deformed axially symmetric Woods–Saxon potential by solving the eigenvalue problem in a space spanned by quasiparticle plus quasiparticle RPA phonon states for each odd nucleus. The calculation, whose details can be found in Refs. 94,194,196,197, is then iterated until a good agreement with the experimental data is reached. Such a procedure fixes the parameters of the potential as well as the quadrupole and hexadecapole deformation parameters β_2 and β_4. The values of all parameters can be found in Refs.93,197. The s.p. spectrum was taken from the bottom of the well up to + 5 MeV.

Two-quasiparticle configurations up to an excitation energy of 30 MeV were taken into account. Monopole and quadrupole pairing were included in the calculation of the quasiparticle energies and amplitudes. The quadrupole pairing was extracted from the $\lambda\mu = 20$ p-p interaction. This term plays an important role in determining the properties of the 0^+ states in deformed nuclei [198]. For a fixed value of its strength G^{20}, the strength of the monopole pairing was determined so as to reproduce the experimental odd-even mass differences. Blocking effect and the Gallagher–Moszkowski corrections [199] were taken into account in computing the two-quasiparticle energies.

The separable interaction includes spin dependent and spin independent p-h multipole terms. The strengths of the spin independent isoscalar p-h interaction terms $\kappa_0^{\lambda\mu}$ were fixed so as to reproduce the lowest experimental energy level for each $K^\pi \neq 1^+$ [194—196]. The only parameters left were the isovector multipole constants and the spin strengths. The first were fixed according to the relation $\kappa_1^{\lambda\mu} = -1.5\kappa_0^{\lambda\mu}$ in substantial agreement with other choices [60]. The spin isoscalar coupling constant was taken to be ten times smaller than the isovector one consistently with the estimates obtained in a sum rule description of spin excitations in heavy spherical nuclei [200]. All parameters used in the study of the $M1$ modes can be found in Ref.93. The only parameter left was the

coupling constant of the isoscalar $\lambda\mu = 21$ Q–Q interaction. This was taken to be slightly larger than a critical value, for which the lowest RPA $K^\pi = 1^+$ state vanishes. With this value the redundant rotational state results to be practically orthogonal to the other intrinsic states. Its overlap with each one of them is less than 0.005.

The basis consists of RPA phonons with $\lambda = 2$–5 multipolarities. Twenty $\lambda\mu = 21$ phonons and ten of the others were included. The $K^\pi = 1^+$ RPA states were computed by including p-h and p-p isoscalar and isovector quadrupole and spin-spin interactions. The $M1$ strength has been calculated by using a spin quenching factor of $g_s = 0.7$.

The $M1$ strength distributions obtained in RPA and QPNM for ^{158}Gd is shown in Fig.4 for illustrative purposes.

From the Figure and from a systematic analysis of the results one may draw the following general conclusions:

i) In each nucleus the RPA calculation yields a strong peak of the order of $(1 \div 1.5)\,\mu_N^2$. Because of the coupling with the two-phonon space this peak splits into two of weaker intensity.

ii) The fragmentation induced by the coupling is otherwise modest. It is appreciable only above 3 MeV. This reflects the fact that the coupling between one- and two-phonon states is weak.

iii) On the whole, the moderate increase in fragmentation improves the agreement with experiments. This can be improved by slight changes of properly chosen parameters. As is shown in the Figure, a change of the strength of the $\lambda\mu = 21$ p-p (pairing) interaction brings sizeable changes on the $M1$ spectrum.

iv) The nature of the transition is not modified by the coupling with the two-phonon states. Most of the strongly excited low-lying QPNM states are dominated by a single RPA phonon. In both RPA and QPNM calculations, practically all transitions are of orbital nature. A modest spin admixture, however, affects considerably the intensity of the transition. In general the spin contribution to the amplitude is additive.

v) The total overlap with the scissors state is 49% in RPA and 45% in QPNM. Most of the other percentage goes to the high-lying states.

vi) The theoretical summed $M1$ strength is larger than the one observed experimentally by a factor $\sim 1.2 \div 1.4$, mainly because of the spin contribution.

vii) As in RPA (see Fig.3), the agreement with experiment would improve drastically if a mechanism leading to a partial suppression of the spin contribution could be found.

The QPNM was also adopted to study magnetic excitations with higher multipoles, in particular the $M3$ transitions [191]. It was found that the spin-octupole isovector interaction plays an important role and shifts the $M3$ strength

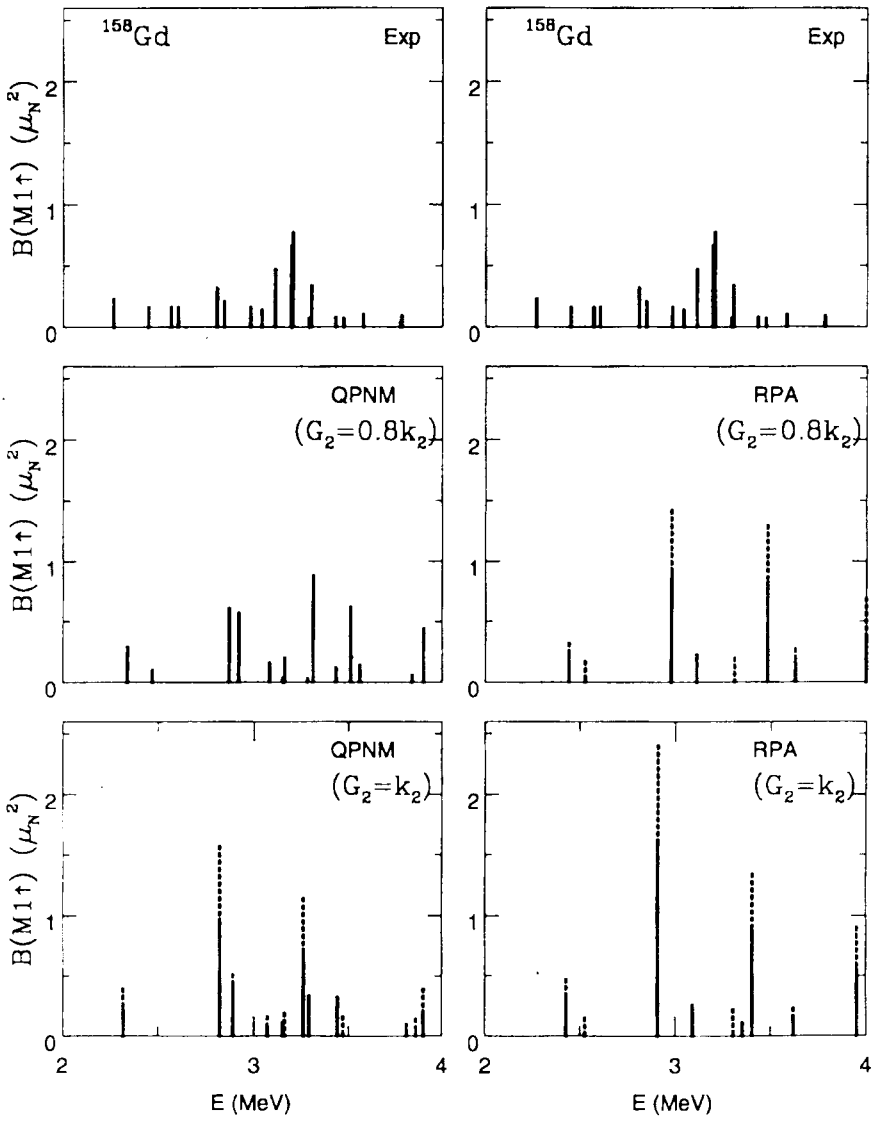

Fig.4. QPNM and RPA $M1$ strength distributions in ^{158}Gd. The full part of each peak gives the orbital strength

up in energy in the region of the isovector magnetic resonances. The $M3$ strength left is fragmented and mainly of spin nature.

7. EXCITATIONS IN ODD-MASS DEFORMED NUCLEI

The question of whether the scissors mode survives as we move from even- to odd-mass nuclei was posed some time ago in studies carried out within the interacting Boson–Fermion model (IBFM) [95,96], in schematic RPA [97] and within the generalized coherent state model (GCSM) [98].

After a first negative attempt [99], dipole transitions which seem to have the properties of the scissors mode have been detected in several odd-mass deformed nuclei of the rare-earth region [20,100,101]. The first experimental search for $M1$ transitions in odd-mass nuclei was carried out in an inelastic electron scattering on ^{165}Ho [99]. No strong $M1$ transition around 3 MeV was found in this nucleus.

Subsequent NRF experiments on ^{163}Dy have detected a sizeable $M1$ strength around 3 MeV which, though more fragmented, fits nicely into the systematic of the scissors mode in the neighboring even-even Dy isotopes [100]. A concentration of dipole strength with the same properties has been found also in other rare-earth nuclei [20] and more recently in ^{167}Er [101]. In this latter experiment, which covered a wider energy range, $1.9 \div 4.3$ MeV, peaks around and above 4 MeV have been detected. The interpretation of these excitations as a manifestation of a scissor-like oscillation mode found support in a theoretical analysis carried out within the IBFM [100,101].

Though appealing, such a response cannot be considered conclusive. In IBFM, in fact, as in all other schematic approaches [97,98], the problem of fragmentation, of crucial importance in odd nuclei, is overlooked.

The theoretical study of $M1$ excitations in odd-nuclei is rendered difficult not only by the extreme fragmentation of some of these spectra, but also by uncertainties inherent in the experimental analysis which will be discussed later. In fact, the polarization techniques, adopted for parity assignment in doubly-even nuclei, are ineffective when applied to odd-mass nuclei. Because of this limitation, the presence of $E1$ excitations intermixed with $M1$ transitions cannot be ruled out. The schematic models are clearly inadequate for clarifying the nature of spectra of such a complexity. One may hope to gain a more clarifying response from microscopic calculations. A fully microscopic calculation which accounts also for the coupling with two-phonon states has been carried out recently [103].

A. With RPA Core States. Equations for describing the nonrotational states in odd-mass deformed nuclei using RPA core state were derived in [201]. These states have the form

$$\Psi_n^{\tau_0}(\sigma_0 K_0^{\pi_0}) =$$

$$= \left\{ \sum_{q_0}^{\tau_0} C_{q_0}^n \alpha_{q_0\sigma_0}^\dagger + \sum_{q_1\sigma_1}^{\tau_0} \sum_{\nu_2\sigma_2} \delta_{\sigma_1 K_1 + \sigma_2\mu_2,\, \sigma_0 K_0} D_{q_1\nu_2}^n \alpha_{q_1\sigma_1}^\dagger Q_{\nu_2\sigma_2}^\dagger \right\} \Psi_0 \qquad (7.1)$$

with the normalization condition

$$\sum_{q_0}^{\tau_0} (C_{q_0}^n)^2 + \sum_{q_1\nu_2}^{\tau_0} (D_{q_1\nu_2}^n)^2 [1 + \mathcal{L}^{K_0}(q_1;\, \nu_2)] = 1. \qquad (7.2)$$

Here the factor

$$\mathcal{L}^{K_0}(q_1;\, \nu_2) = -\sum_{q_2} (\psi_{q_1 q_2}^{\nu_2})^2 \qquad (7.3)$$

comes from antisymmetrizing the quasiparticle-phonon components of (7.1). This has been done for the first time in Ref.202. Using the above wave function one deduces energies and eigenvectors from the variational principle. They can be found in Ref.94.

B. With QPNM Core States. As shown in [93,195,203], at energies above 2.5 MeV the coupling with the two-phonon configurations induces fragmentation of the $K^\pi = 1^+$ and $K^\pi = 0^-,\ 1^-$ modes in doubly-even nuclei. Being interested in the distribution of the magnetic and electric transitions falling in the energy range (2.5—3.5) MeV, we need to take such a two-phonon coupling into account also in odd-mass nuclei. The mathematical procedure developed in [204] is followed. The basic idea is to use the already fragmented phonons in the wave function of excited states according to the procedure described by eqs.(4.86)—(4.90) in [94]. To this purpose the following trial wave function is chosen

$$\Psi_n^{\tau_0}(\sigma_0 K_0^{\pi_0}) = \left[\sum_{q_0}^{\tau_0} C_{q_0}^n \alpha_{q_0\sigma_0}^\dagger + \sum_{q_1\sigma_1}^{\tau_0} \sum_{\substack{\nu_2\sigma_2 \\ \lambda_2\mu_2 \neq \bar{\lambda}\bar{\mu}}} \delta_{\sigma_1 K_1 + \sigma_2\mu_2,\, \sigma_0 K_0} D_{q_1\nu_2}^n \alpha_{q_1\sigma_1}^\dagger Q_{\nu_2\sigma_2}^\dagger + \right.$$

$$\left. + \sum_{q_3\sigma_3}^{\tau_0} \sum_{\bar{n}\,\bar{\sigma}} \delta_{\sigma_3 K_3 + \bar{\sigma}\,\bar{\mu},\, \sigma_0 K_0} \overline{D}_{q_3\bar{\lambda}\bar{\mu}\,\bar{n}}^{\,n} \alpha_{q_3\sigma_3}^\dagger \Omega_{\bar{\lambda}\,\bar{\mu}\,\bar{n}\,\bar{\sigma}}^\dagger \right] \Psi_0 \qquad (7.4)$$

with the normalization condition

$$\sum_{q_0}^{\tau_0} (C^n_{q_0})^2 + \sum_{\substack{q_1\nu_2 \\ \lambda_2\mu_2 \neq \bar{\lambda}\bar{\mu}}}^{\tau_0} (D^n_{q_1\nu_2})^2[1 + \mathcal{L}^{K_0}(q_1; \nu_2)] + \sum_{q_3\bar{n}}^{\tau_0} (\bar{D}^n_{q_3\bar{\lambda}\bar{\mu}\bar{n}})^2 = 1. \quad (7.5)$$

The QPNM core states have the quantum numbers $\{\bar{n}, \bar{\lambda} = 2, \bar{\mu} = 1\}$ for the $M1$ excitations and $\{\bar{n}, \bar{\lambda} = 3, \bar{\mu} = 0\}$ or $\{\bar{n}, \bar{\lambda} = 3, \bar{\mu} = 1\}$ for the $\Delta K = 0$ or $\Delta K = 1$ $E1$ transitions respectively.

Under the assumption

$$[\alpha_{q\sigma}, \Omega^{\dagger}_{\nu}] = 0 \quad (7.6)$$

which is a valid approximation when the energy of the core states is above 2.5 MeV, a variational calculation yields a secular equation whose rank equals the number of one-quasiparticle states of the wave function (7.4).

The $E1$ and $M1$ transition probabilities were computed by using the total wave function

$$\Psi^I_{nMK^{\pi}\sigma} = \sqrt{\frac{2I+1}{16\pi^2}} [D^I_{MK}\Psi_{nK^{\pi}\sigma} + (-1)^{I+K} D^I_{M-K}\Psi_{nK^{\pi}-\sigma}]. \quad (7.7)$$

For the reduced $E1$ transition probabilities an effective charge

$$e^{(1)}_{\text{eff}}(\tau_z) = -\frac{e}{2}\left(\tau_z - \frac{N-Z}{A}\right)(1 + \chi). \quad (7.8)$$

The factor χ is a fitting parameter introduced to quench the too large $E1$ transition probabilities obtained with the standard expression ($\chi = 0$). For the $M1$ reduced strength a bare orbital gyromagnetic factor and an effective spin factor $g_s^{\text{eff}} = 0.7 g_s^{\text{free}}$ were used. Given the impossibility of distinguishing experimentally between $E1$ and $M1$ transitions in odd-mass nuclei, it is appropriate to compute the widths, multiplied by the statistical factor $g = (2I_f + 1)/(2I_0 + 1)$. These quantities are in fact parity and spin independent and are related to the reduced strengths according to

$$g\Gamma_0(E1) = 1.0467(E_{\gamma}[\text{MeV}])^3 \text{B}(E1) \uparrow [\text{e}^2\text{fm}^2 10^{-3}] \text{ meV},$$

$$g\Gamma_0(M1) = 11.547(E_{\gamma}[\text{MeV}])^3 \text{B}(M1) \uparrow [\mu_N^2] \text{ meV}. \quad (7.9)$$

A more closely related quantity is represented by the reduced widths

$$g\Gamma_0^{\text{red}}(E1) = 1.0467 \text{B}(E1) \uparrow [\text{e}^2\text{fm}^2 10^{-3}] \text{ meV (MeV)}^{-3},$$

$$g\Gamma_0^{\text{red}}(M1) = 11.547 \text{B}(M1) \uparrow [\mu_N^2] \text{ meV (MeV)}^{-3}. \quad (7.10)$$

The phonons of different multipolarity were calculated using isoscalar and isovector interactions embodying the appropriate multipole fields. The phonon basis consists of ten (i = 1,2,... 10) phonons of a given multipolarity: $\lambda\mu$ = 20, 22, 32, 33, 43, 44, 54 and 55. Twenty-five (i = 1, 2,..., 25) phonons of $\lambda\mu$ = 21 and $\lambda\mu$ = 30 and 31 multipolarities were used. The same phonon basis was used for doubly-even and odd-mass nuclei.

Numerical calculations were carried out for ^{157}Gd, ^{159}Tb, ^{161}Dy, ^{163}Dy and ^{167}Er. The core states entering into the quasiparticle-phonon basis are respectively the states of ^{156}Gd, ^{158}Gd, ^{160}Dy, ^{162}Dy and ^{166}Er.

1. M1 Transitions. In going from even- to odd-nuclei the fragmentation of the strength is dramatically enhanced. This phenomenon is illustrated in Fig.5 showing the $M1$ spectra computed within RPA and QPNM for ^{162}Dy and ^{163}Dy. The spectrum of the odd-mass nucleus is much richer than in the case of the doubly-even one. A further increase in fragmentation is observed when the $M1$ core states are computed in QPNM rather than RPA.

That the strength should get strongly fragmented in going from doubly-even to odd-mass nuclei was largely expected. On the one hand, the quasiparticle $\otimes$ $(\lambda\bar{\mu})_i$ components couple to several one-quasiparticle configurations. As a rule, the fragmentation so induced is rather weak due to the small number of one-quasiparticle states. On the other hand, the strength collected by each $M1$ state in a doubly-even nucleus is distributed among four $M1$ levels in the neighboring odd-mass nucleus. In this latter system, in fact, the $M1$ operator can couple the $\{K_0, I_0 = K_0\}$ ground state to a multiplet of four excited states with quantum numbers $\{(K_0 - 1, I_0 - 1), (K_0 - 1, I_0), (K_0 - 1, I_0 + 1)\}$ and $\{K_0 + 1, I_0 + 1\}$.

Let us study this problem more quantitatively by analyzing the results obtained for ^{163}Dy. The strength of the strongest $M1$ transition occurring in ^{162}Dy at an excitation energy E = 2.90 MeV and estimated to be $B(M1)\uparrow \simeq$ $\simeq 0.90\mu_N^2$ is distributed in ^{163}Dy almost equally among the $K_f^\pi = 3/2^-$ and $K_f^\pi = 7/2^-$ levels, both having an intrinsic excitation energy 2.89 MeV. The two K_f^π states, indeed, collect respectively

$$\sum_{I_f^\pi} B(M1)\left(K_i^\pi = I_i^\pi = \frac{5^-}{2} \rightarrow K_f^\pi = \frac{3^-}{2}\ I_f^\pi\right) \simeq 0.45\mu_N^2,$$

$$B(M1)\left(K_i^\pi = I_i^\pi = \frac{5^-}{2} \rightarrow K_f^\pi = I_f^\pi = \frac{7^-}{2}\right) \simeq 0.47\,\mu_N^2.$$

The $K_f^\pi = 3/2^-$ strength, however, is further distributed among the $I_f^\pi = 3/2^-$, $5/2^-$, $7/2^-$ states with strengths $B(M1) \simeq 0.30$, 0.13, $0.02\,\mu_N^2$, respectively.

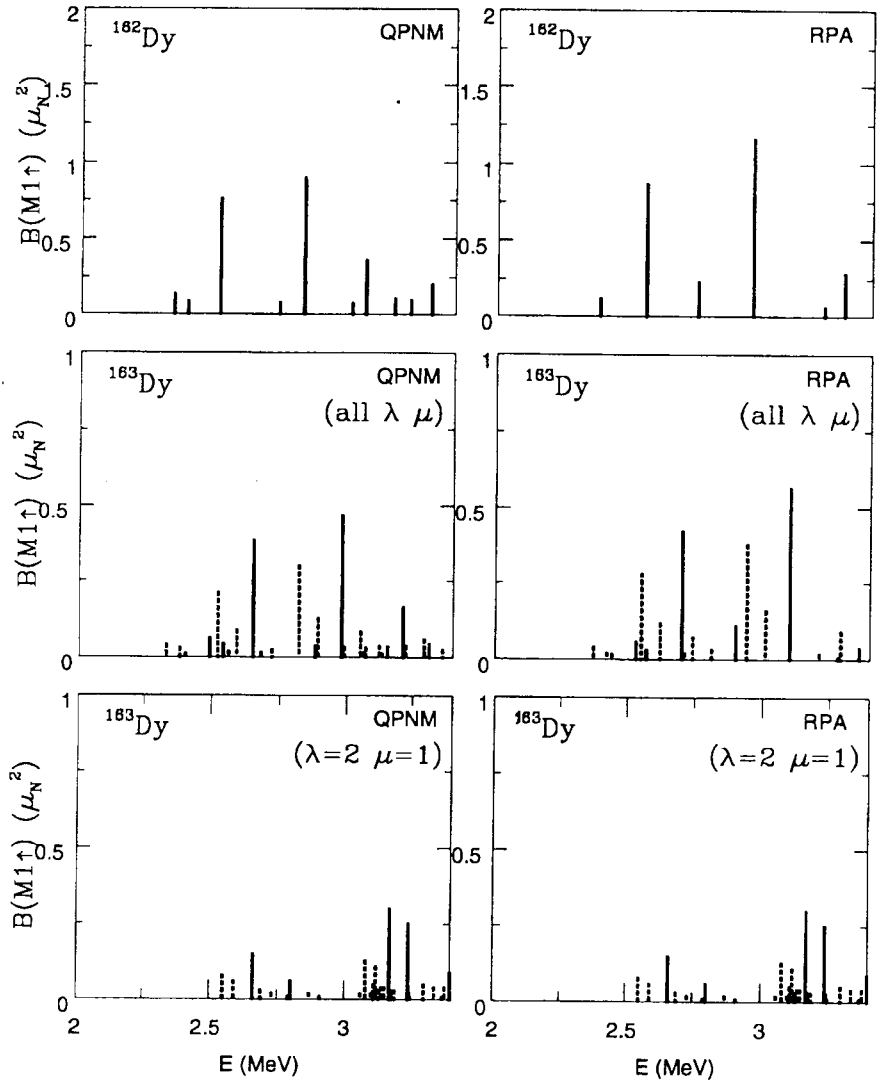

Fig.5. QPNM and RPA $M1$ strength distributions in ^{162}Dy and ^{163}Dy. Full and dotted lines refer respectively to transitions to $K_f = 3/2$ and $K_f = 7/2$ final states

The $I_f^\pi = 3/2^-$ state gets about 2/3 of the strength. That the $I_f^\pi = K_f^\pi$ states take 2/3 of the K_f^π strength is a general feature to be ascribed to angular momentum coupling.

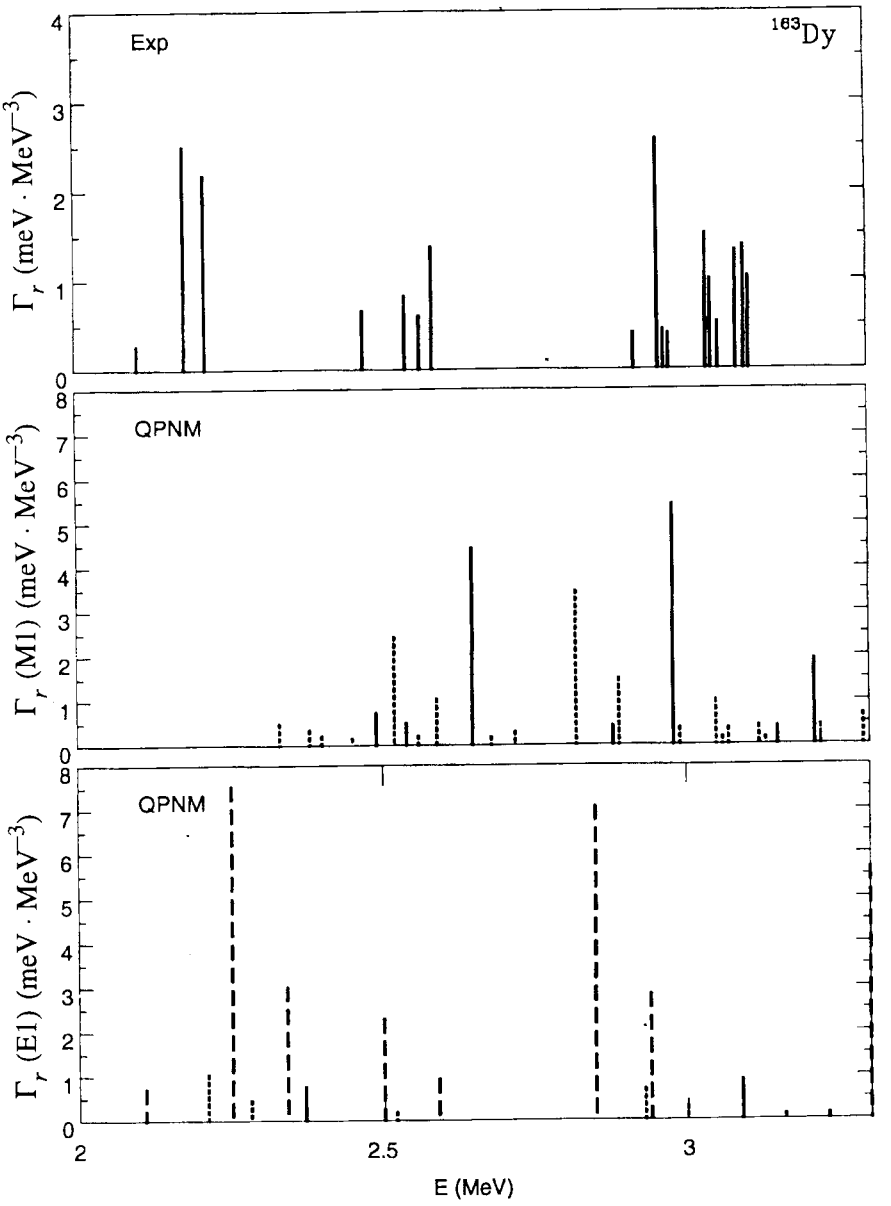

Fig.6. Ground state decay reduced width distribution in ^{163}Dy. Full, dashed and dotted lines refer respectively to $K_f = 3/2,\ 5/2,\ 7/2$ final state

The states collecting appreciable amounts of $M1$ strength are dominated by a single quasiparticle-phonon configuration obtained by coupling the valence quasiparticle to the $(\bar{\lambda}\bar{\mu}) = 21$ phonon. The effect of the substantial purity of the $M1$ states is illustrated in the lower part of Fig.5 showing the $M1$ strength distributions when only the $(\bar{\lambda}\bar{\mu})$ are included in the calculation. This is what is done in schematic approaches [97]. The spectrum so obtained is quite similar to the corresponding one deduced from including all core states.

The spectra of the reduced widths of ^{163}Dy, computed in QPNM, are compared with the experimental data in Fig.6. The following points are noteworthy: i) The computed $M1$ transitions fall in the region of the observed peaks in all nuclei. The discrepancies in the energy distribution with respect to experiments are of the same order as in the nearby doubly-even nuclei. ii) The $K^\pi \to K^\pi + 1$ $M1$ transitions are fewer but in general much stronger than in the $K^\pi \to K^\pi - 1$ case. As already said for ^{163}Dy, the $M1$ strength of the neighboring doubly-even nuclei is equally shared by the two K_f^π states, but for $K_f^\pi = K_i^\pi - 1$ the strength is further distributed mostly among two out of the three J_f components of the K_f^π multiplet. iii) The magnitude of the strongest $M1$ peaks is about twice the intensity of the corresponding observed transitions. Also the summed reduced widths are in general about twice the experimental values.

2. E1 Transitions. In odd-mass nuclei the fragmentation mechanism of the $\Delta K = \pm 1$ $E1$ strength is obviously the same as for the $M1$ transitions. Exactly as in the case of the $M1$ transitions, the $\Delta K = 1$ $E1$ strength is also equally shared by the $K_f^\pi = K_f^\pi - 1$ and $K_f^\pi = K_f^\pi + 1$ levels and the $I_f^\pi = K_f^\pi$ states take 2/3 of the K_f^π strength. However, as in doubly-even nuclei [193], the $\Delta K = 1$ $E1$ strength represents a small fraction of the total transition probability. This is mostly concentrated in the $\Delta K = 0$ transitions. These transitions are in general more than 5 times stronger. As in the $M1$ case, the $E1$ states have a dominant configuration embodying the $(\bar{\lambda}\bar{\mu})$ phonon.

Figure 6 shows that the $M1$ widths are much larger than the corresponding $\Delta K = 1$ $E1$ widths. Indeed, as in the doubly-even nuclei, the $E1$ strength is concentrated almost entirely in the $\Delta K = 0$ transitions. These can be quite strong. The strongest peaks are larger than the magnetic transitions and more than 3 times the experimental widths. These strong $E1$ transitions correspond to strong $E1$ excitations of collective octupole core states. However, no strong $E1$ transitions above 2 MeV have been observed in the nearby doubly-even nuclei. One could reduce the strength of these transitions by using a smaller effective charge, as done in Ref. 205. This new effective charge, however, would quench

also the low-lying $E1$ transitions thereby spoiling the agreement with experiments. This is an unsolved problem yet, which requires detailed specific studies.

We can conclude that the occurrence of $E1$ transitions of appreciable strength in the observation region cannot be ruled out but cannot be assessed with certainty due to the discrepancies between theory and experiments found in the doubly-even nuclei for these transitions. On the other hand, the $M1$ and $E1$ transitions are predicted to carry different ΔK quantum numbers. More refined experiments may hopefully exploit this fact in order to settle upon the exact nature of the observed widths. In any case, the problem of reproducing the extreme fragmentation of the $M1$ strength, specially in some nuclei like ^{157}Gd, remains unsolved.

8. CONCLUSIONS

We have seen that the collective features of the low-lying $M1$ excitations, chiefly the quadratic deformation law, are described fairly well in several phenomenological approaches. All these models have been shown to be mutually correlated. They can actually be put within a unified context having the TRM as the common root. Each of them can be indeed turned into TRM-like models when the variables which describe the shapes oscillations of the nuclei are frozen. The differences among them are to be attached mainly to the different microscopic structure underlying each model. While in fact the IBM boson operators are to be considered as highly correlated valence fermion pairs, in the other two interacting boson models under investigations (NPD and GCSM) the bosons should be viewed, at least in lowest order, as highly correlated p-h fermion states. The microscopic counterpart of IBM is therefore the standard shell model, while RPA is the microscopic scheme underlying the other Boson models. We have shown that in their schematic version both shell-model and RPA are intimately related to the TRM and actually provide the tools for computing the TRM quantities in a realistic way.

In going from schematic to realistic RPA descriptions the correspondence with the TRM as well as with the other phenomenological models is far from appearing obvious. Because of the extreme fragmentation of the two-quasiparticle spectrum the naive HO picture with one single degenerate p-h level seems therefore quite far from reality. It is rewarding that because of the spin-spin interaction which pushes the spin excitations up in energy, the quadrupole pairing which rearranges the $M1$ strength distribution among different p-h levels and the recoil term, the fragmentation is drastically reduced.

The many RPA calculations carried out since the discovery of the mode have shown that such a mode is extremely sensitive to the choice of the s.p. energy and of the two-body interaction as well as to the approximations invol-

ved. Because of this extreme sensitivity, the calculations had to meet certain requirements. A major one was the removal of the redundant rotational mode from the physical $M1$ states. This problem has been clearly illustrated here and a simple prescription for its solution has been given. All recent RPA calculations are free from this problem and tend toward converging results. Indeed, all of them agree in interpreting the low-lying $M1$ peaks around 3 MeV as the signature of a scissors like rotational oscillation between proton and neutron deformed fluids. The simple TRM picture appears therefore valid. Only one should think of a rotational oscillation between two superfluids rather than two rigid bodies or two normal irrotational fluids.

The only point which is still under debate is the collective character of the mode. We observe in this respect that the collectivity of this $M1$ excitation should not be «measured» in terms of s.p. units as for instance in the case of the $E1$ or $E2$ giant resonances. The mode under study here, arises in fact from deformation and disappears as deformation is turned off. This emerges nicely from the δ^2 dependence of the $M1$ strength. A more sensitive test of the collectivity of the mode is provided by the $M1$ energy weighted sum rule. Recent calculations [185] show that the observed strength is short from exhausting such a sum rule. A strong indication in this respect is further provided by the fact that the excitation is observed throughout all deformed (light and heavy) nuclei and its strength goes smoothly with deformation.

The RPA descriptions are not able to reproduce faithfully the $M1$ energy spectrum. A progress in this direction has been achieved by going beyond RPA. This has been done by accounting for the coupling with the two-phonon RPA state within the QPNM. Even this extension seems not sufficient. It is to be pointed out however that the calculations carried out in this context are parameter free calculations. Minor adjustments may improve the agreement with experiments considerably.

One of the most exciting recent discoveries was the detection of $M1$ excitations exhibiting the properties of the scissors mode in odd-mass nuclei but with a much more fragmented strength. The only microscopic thorough description of these spectra has been carried out recently in QPNM. Many aspects have been clarified. Many problems remain unsettled. The calculation in fact indicates that the occurrence of $E1$ excitations intermixed with $M1$ transitions cannot be ruled out. It also indicates that the detected total strength is quite smaller than that predicted by the calculations. Moreover, the extreme fragmentation observed in some nuclei remains an unexplained puzzle.

Let us now move to future perspectives. It is of great interest the possible occurrence of a high energy mode of scissors nature. The sharing of the $M1$ strength among a low and a high energy modes is reminiscent of the isoscalar $E2$ strength known to be concentrated in a high and a low energy modes. The detection of such a mode is related to the discovery of the $E2$ isovector giant resonance in deformed nuclei.

Strongly excited $M1$ excitations of scissors nature both at low and high energy are predicted also for superdeformed nuclei. Whether these modes can be observed directly is an open question.

The perspective of finding the mode in γ-soft nuclei is becoming a reality. Pursuing in the search for $M3$ transitions would help to complete the picture.

We like to conclude by saying that the occurrence of orbital $M1$ excitations has uncovered a beautiful example of dynamical symmetry in nuclei and has provided a unique and sensitive test ground for many phenomenological models as well as for microscopic theories. From its extensive study we have tested effective interactions and correlations among nucleons in nuclei and we have enriched considerably our knowledge on the low energy nuclear properties.

REFERENCES

1. **Bohle D., Richter A., Steffen W. et al.** — Phys. Lett., 1984, v.B137, p.27.
2. **Lo Iudice N., Palumbo F.** — Phys. Rev. Lett., 1978, v.41, p.1532;
   De Franceschi G., Palumbo F., Lo Iudice N. — Phys. Rev., 1984, v.C29, p.1496.
3. **Iachello F.** — Nucl. Phys. 1981, v.A358, p.89c.
4. **Dieperink A.E.L.** — Prog. Part. Nucl. Phys., 1983, v.9, p.121.
5. **Hilton R.R.** — Z. Phys., 1984, v.A316, p.121.
6. **Richter A.** — Nucl. Phys., 1990, v.A507, p.99c; 1991, v.A522, p.139c; Nucl. Phys. 1992, v.A553, p.417c.
7. **von Brentano P., Zilges A., Heil R.D. et al.** — Nucl. Phys., 1993, v.A557, p.593c.
8. **Richter A.** — Prog. Part. Nucl. Phys., 1995, v.34, p.261.
9. **Kneissl U., Margraf J., Pitz H.H. et al.** — Prog. Part. Nucl. Phys., 1995, v.34, p.285.
10. **Kneissl U., Pitz H.H., Zilges A.** — Prog. Part. Nucl. Phys., 1996, v.37, p.349.
11. **Ziegler W., Rangacharyulu C., Richter A., Spieler C.** — Phys. Rev. Lett., 1990, v.65, p.2515.
12. **Rangacharyulu C., Richter A., Wörtche H.J. et al.** — Phys. Rev., 1991, v.C43, p.R949.
13. **Margraf J., Heil R.D., Kneissl U. et al.** — Phys. Rev., 1993, v.C47, p.1474.
14. **von Brentano P., Zilges A., Herzberg R.-D. et al.** — Nucl. Phys., 1994, v.A577, p.191c and references therein.
15. **Pietralla N., von Brentano P., Herzberg R.-D. et al.** — Phys. Rev., 1995, v.C52, p.R2317.
16. **Heil R.D., Kasten B., Scharfe W. et al.** — Nucl. Phys., 1990, v.A506, p.223.
17. **Friedrichs H., Schlitt B., Margraf J. et al.** — Phys. Rev., 1992, v.C45, p.R892.
18. **Zilges A., von Brentano P., Friedrichs H. et al.** — Z. Phys., 1991, v.A340, p.155.
19. **Friedrichs H., Häger D., von Brentano P. et al.** — Nucl. Phys., 1994, v.A567, p.266.
20. **Margraf J., Eckert T., Rittner M. et al.** — Phys. Rev., 1995, v.C52, p.2429.
21. **Frekers D., Wörtche H.J., Richter A. et al.** — Phys. Lett., 1990, v.B244, p.178.
22. **Richter A.** — Nucl. Phys., 1993, v.A553, p.417c.
23. **Van Isacker P., Heyde K., Waroquier M. et al.** — Phys. Lett., 1984, v.B144, p.1.

24. **Scholten O., Dieperink A.E.L., Heyde K., Van Isacker P.** — Phys. Lett., 1984, v.B149, p.279.
25. **Pittel S., Dukelsky J., Perazzo R.P.J., Sofia H.M.** — Phys. Lett., 1984, v.B144, p.145.
26. **Otsuka T., Ginocchio J.N.** — Phys. Rev. Lett., 1985, v.54, p.777.
27. **Scholten O., Heyde K., Van Isacker P.** — Nucl. Phys., 1985, v.A438, p.41.
28. **Barrett B.R., Halse P.** — Phys. Lett., 1985, v.B155, p.133.
29. **Van Isacker P., Heyde K., Jolie J., Sevrin A.** — Ann. Phys., 1986, v.171, p.253 and references therein.
30. **Faessler A., Nojarov R.** — Phys. Lett., 1986, v.B166, p.367;
Nojarov R., Bochnacki Z., Faessler A. — Z. Phys.,1986, v.A324, p.289;
Faessler A., Bochnacki Z., Nojarov R. — J. Phys., 1986, v.G12, p.L47.
31. **Rohozinski S.G., Greiner W.** — Z. Phys., 1985, v.A322, p.271.
32. **Raduta A.A., Faessler A., Ceasescu V.** — Phys. Rev., 1987, v.C36, p.2111.
33. **Raduta A.A., Ursu I.I., Delion D.S.** — Nucl. Phys., 1987, v.A475, p.439.
34. **Lipparini E., Stringari S.** — Phys. Lett., 1983, v.B130, p.139.
35. **Suzuki T., Rowe D.J.** — Nucl. Phys., 1977, v.A289, p.461.
36. **Bes D.R., Broglia R.A.** — Phys. Lett., 1984, v.B137, p.141.
37. **Kurasawa H., Suzuki T.** — Phys. Lett. 1984, v.B144, p.151.
38. **Dieperink A.E.L., Moya de Guerra E.** — Phys. Lett., 1987, v.B189, p.267.
39. **Zamick L.** — Phys. Rev., 1985, v.C31, p.1955; Phys. Lett. 1986, v.B167, p.1; Phys. Rev., 1986, v.C33, p.691.
40. **Liu H., Zamick L.** — Phys. Rev., 1987, v.C36, p.2057; 1987, v.C36, p.2064; Nucl. Phys., 1987, v.A467, p.29.
41. **Castel B., Zamick L.** — Phys. Rep., 1987, v.148, p.217.
42. **Zamick L., Zheng D.C.** — Phys. Rev., 1991, v.C44, p.2522; 1992, v.C46, p.2106.
43. **Abdelaziz M., Thompson M.J., Elliot J.P., Evans J.A.** — J. Phys. G: Nucl. Phys., 1988, v.14, p.219.
44. **Abdelaziz M., Thompson M.J., Elliot J.P., Evans J.A.** — Nucl. Phys., 1989, v.A503, p.452.
45. **Chaves L., Poves A.** — Phys. Rev., 1986, v.C34, p.1137.
46. **Poves A., Retamosa J., Moya de Guerra E.** — Phys. Rev., 1989, v.C39, p.1356.
47. **Retamosa J., Udias J.M., Poves A., Moya de Guerra E.** — Nucl. Phys., 1990, v.A511, p.221.
48. **Castaños O., Draayer J.P., Leschber Y.** — Nucl. Phys., 1987, v.A473, p.494.
49. **Castaños O., Draayer J.P., Leschber Y.** — Ann. Phys., 1987, v.A180, p.290.
50. **Hammaren E., Schmid K.W., Faessler A., Grümmer F.** — Phys. Lett., 1986, v.B171, p.347.
51. **Hammaren E., Heikkinen P., Schmid K.W., Faessler A.** — Nucl. Phys., 1992, v.A541, p.226.
52. **Iwasaki S., Hara K.** — Phys. Lett., 1984, v.B144, p.9.
53. **Hamamoto I., Åberg S.** — Phys. Lett., 1984, v.B145, p.163.
54. **Hamamoto I., Åberg S.** — Physica Scripta, 1986, v.34, p.697.
55. **Hilton R.R., Iwasaki S., Mang H.J. et al.** — In: Microscopic Approaches to Nuclear Structure Calculations, ed. A. Covello, Editrice Compositori-Bologna, 1986, p.357.
56. **Hamamoto I., Rönstrom C.** — Phys. Lett., 1987, v.B194, p.6.
57. **Civitarese O., Faessler A., Nojarov R.** — Phys. Rev., 1987, v.C35, p.2310.

58. **Nojarov R., Faessler A., Civitarese O.** — Phys. Lett., 1987, v.B183, p.122.
59. **Speth J., Zawischa D.** — Phys. Lett., 1988, v.B211, p.247; Phys. Lett., 1989, v.B219, p.229.
60. **Nojarov R., Faessler A.** — Nucl. Phys., 1988, v.A484, p.1.
61. **Sugawara-Tanabe K., Arima A.** — Phys. Lett., 1988, v.B206, p.573.
62. **Scholtz F.G., Nojarov R., Faessler A.** — Phys. Rev. Lett., 1989, v.63, p.1356.
63. **Faessler A., Nojarov R.** — Phys. Rev., 1990, v.C41, p.1243.
64. **Nojarov R., Faessler A.** — Z. Phys., 1990, v.A336, p.151.
65. **Faessler A., Nojarov R., Scholtz F.G.** — Nucl. Phys., 1990, v.A515, p.237.
66. **Faessler A., Khoa D.T., Grigorescu M., Nojarov R.** — Phys. Rev. Lett., 1990, v.65, p.2978.
67. **Zawischa D., Macfarlane M., Speth J.** — Phys Rev., 1990, v.C42, p.1461.
68. **Zawischa D., Speth J.** — Phys. Rev. Lett., 1990, v.B252, p.4.
69. **Hamamoto I., Magnusson C.** — Phys. Lett., 1991, v.B260, p.6.
70. **Magnusson C.** — Physica Scripta, 1991, v.43, p.460.
71. **Nojarov R., Faessler A., Lipas P.O.** — Nucl. Phys., 1991, v.A553, p.381; 1992, v.A537, p.707.
72. **Hamamoto I., Nazarewicz W.** — Phys. Lett., 1992, v.B297, p.25.
73. **Nojarov R., Faessler A., Sarriguren P.,** — Nucl. Phys., 1993, v.A563, p.349.
74. **Sarriguren P., Moya de Guerra E., Nojarov R., Faessler A.** — J. Phys: Nucl. Phys., 1993, v.G19, p.291; 1994, v.G20, p.315.
75. **Nojarov R., Faessler A.** — Nucl. Phys., 1994, v.A572, p.17.
76. **Nojarov R., Faessler A., Dingfelder M.** — Phys. Rev., 1995, v.C51, p.2449.
77. **Raduta A.A., Lo Iudice N., Ursu I.I.** — Nucl. Phys., 1995, v.A584, p.84.
78. **De Coster C., Heyde K.** — Nucl. Phys., 1991, v.A529, p.507.
79. **Heyde K., De Coster C.** — Phys. Rev., 1991, v.C44, p.R2262.
80. **Garrido E., Moya de Guerra E., Sarriguren P., Udias J.M.** — Phys. Rev., 1991, v.C44, R1250.
81. **Moya de Guerra E., Zamick L.** — Phys. Rev., 1993, v.C47, p.2604.
82. **Hilton R.R., Höhenberger W., Mang H.J.** — Phys. Rev., 1993, v.C47, p.602.
83. **Smith B.H., Pan X.W., Feng D.H., Guidry M.** — Phys. Rev. Lett., 1995, v.75, p.3086.
84. **Ginocchio J.N.** — Phys. Lett., 1991, v.B265, p.6.
85. **Mizusaki T., Otsuka T., Sugita M.** — Phys. Rev., 1991, v.C44, p.R1277.
86. **Heyde K., De Coster C., Richter A., Wörtche H.-J.** — Nucl. Phys., 1992, v.A549, p.103.
87. **Heyde K., De Coster C., Ooms D., Richter A.** — Phys. Lett., 1993, v.B312, p.267.
88. **Heyde K., De Coster C., Ooms D.** — Phys. Rev., 1994, v.C49, p.156.
89. **Lo Iudice N., Raduta A.A., Delion D.S.** — Phys. Lett., 1993, v.B300, p.195; Phys. Rev., 1994, v.C50, p.127.
90. **Lo Iudice N., Richter A.** — Phys. Lett., 1993, v.B304, p.193.
91. **von Neumann-Cosel P., Ginocchio J.N., Bauer H., Richter A.** — Phys. Rev. Lett., 1995, v.75, p.4178.
92. **Lo Iudice N.** — Phys. Rev., 1996, v.C53, p.2171.
93. **Soloviev V.G., Sushkov A.V., Shirikova N.Yu., Lo Iudice N.** — Nucl. Phys., 1996, v.A600, p.155.

94. **Soloviev V.G.** — Theory of Atomic Nuclei: Quasiparticles and Phonons, Institute of Physics, Bristol and Philadelphia, 1992.
95. **Van Isacker P., Frank A.** — Phys. Lett., 1989, v.B225, p.1.
96. **Frank A., Arias J.M., Van Isacker P.** — Nucl. Phys., 1991, v.A531, p.125.
97. **Raduta A.A., Lo Iudice N.** — Z. Physik, 1989, v.A334, p.403.
98. **Raduta A.A., Delion D.S.** — Nucl. Phys., 1990, v.A513, p.11.
99. **Huxel N., Ahner W., Diesener H. et al.** — Nucl. Phys., 1992, v.A539, p.478.
100. **Bauske I., Arias J.M., von Brentano P. et al.** — Phys. Rev. Lett., 1993, v.71, p.975.
101. **Schlegel C., von Neumann-Cosel P., Richter A., Van Isacker P.** — Phys. Lett., 1996, v.B375, p.21.
102. **Soloviev V.G., Sushkov A.V., Shirikova N.Yu.** — Phys. Rev., 1996, v.C53, p.1022.
103. **Soloviev V.G., Sushkov A.V., Shirikova N.Yu., Lo Iudice N.** — Nucl. Phys., 1997, v.A613, p.1.
104. **Goldhaber M., Teller E.** — Phys. Rev., 1948, v.73, p.1156.
105. **Steinwedel H., Jensen J.H.D.** — Z. Naturforschung, 1950, v.5a, p.413.
106. **Lo Iudice N.** — Phys. Rev., 1986, v.C34, p.1501.
107. **Bohle D., Kilgus G., Richter A. et al.** — Phys. Lett., 1987, v.B195, p.326.
108. **Richter A.** In: Contemporary Topics in Nuclear Structure Physics, eds. R.F.Casten, A.Frank, M.Moshinsky and S. Pittel, World Scientific, Singapore 1988, p.127.
109. **Berg U.E.P., Bläsing C., Drexler J. et al.** — Phys. Lett., 1984, v.B149, p.59.
110. **Alaga G., Alder K., Bohr A., Mottelson B.R.** — Dan. Mat. Fys. Medd., 1955, v.29, No.9, p.1.
111. **Bohle D., Küchler G., Richter A., Steffen W.** — Phys. Lett., 1984, v.B148, p.260.
112. **Wesselborg C., von Brentano P., Zell K.O. et al.** — Phys. Lett., 1988, v.B207, p.22.
113. **Hartmann U., Bohle D., Humbert F., Richter A.** — Nucl. Phys., 1989, v.A499, p.93.
114. **Pitz H.H., Berg U.E.P., Heil R.D. et al.** — Nucl. Phys., 1989, v.A492, p.411.
115. **Kasten B., Heil R.D., von Brentano P. et al.** — Phys. Rev. Lett., 1989, v.63, p.609.
116. **Pitz H.H., Heil R.D., Kneissl U. et al.** — Nucl. Phys., 1990, v.A509, p.587.
117. **Zilges A., von Brentano P., Wesselborg C. et al.** — Nucl. Phys., 1990, v.A507, p.399.
118. **Herzberg R.-D., Zilges A., von Brentano P. et al.** — Nucl. Phys., 1993, v.A563, p.445.
119. **Maser M., Lindenstruth S., Bauske I. et al.** — Phys. Rev., 1996, v.C53, p.2749.
120. **Djalali C., Marty N., Morlet M. et al.** — Phys. Lett., 1985, v.B164, p.269.
121. **Richter A.** — Prog. Part. Nucl. Phys., 1985, v.13, p.1.
122. **Degener A., Bläsing C., Heil R.D. et al.** — Nucl. Phys., 1990, v.A513, p.29.
123. **Heil R.D., Pitz H.H., Berg V.E.P. et al.** — Nucl. Phys., 1988, v.A476, p.39.
124. **Margraf J., Degener A., Friedrichs H. et al.** — Phys. Rev., 1990, v.C42, p.771.
125. **Wesselborg C., Schiffer K., Zell K.O. et al.** — Z. Phys., 1986, v.A323, p.485.
126. **Frekers D., Bohle D., Richter A. et al.** — Phys. Lett., 1989, v.B218, p.439.
127. **Bohle D., Richter A., Berg U.E.P. et al.** — Nucl. Phys., 1986, v.A458, p.205.
128. **Freeman S.J., Chapman R., Durell J.L. et al.** — Phys. Lett., 1988, v.B222, p.347.
129. **Freeman S.J., Chapman R., Durell J.L. et al.** — Nucl. Phys., 1993, v.A554, p.333.
130. **Margraf J., Wesselborg C., Heil R.D. et al.** — Phys. Rev., 1992, v.C45, p.R521.
131. **von Brentano P., Eberth J., Enders J. et al.** — Phys. Rev. Lett., 1996, v.76, p.2029.
132. **Maser M., Pietralla N., von Brentano P. et al.** — Phys. Rev.,1996, v.C54, p.1.

133. **Bohr A., Mottelson B.R.** — Nuclear Structure, Benjamin, N. Y., Vol.II, 1975, ch.6.
134. **Lo Iudice N.** — In «Capture Gamma-Ray Spectroscopy», ed. J.Kern, World Scientific, Singapore 1994, p.154.
135. **Palumbo F., Richter A.** — Phys. Lett., 1985, v.B158, p.101.
136. **Lo Iudice N., Lipparini E., Stringari S. et al.** — Phys. Lett., 1985, v.B161, p.18.
137. **Nojarov R.** — Nucl. Phys., 1994, v.A571, p.93.
138. **Faessler A.** — Nucl. Phys., 1966, v.85, p.653.
139. **Rohozinski S.G., Troltenier D., Maruhn J.A., Greiner W.** — Z. Phys., 1988, v.A330, p.23.
140. **Raduta A.A., Ceasescu V., Gheorghe A., Dreizler R.M.** — Phys. Lett., 1981, v.B99, p.444; Nucl. Phys., 1982, v.A381, p.253.
141. **Raduta A.A., Delion D.S.** — Nucl. Phys., 1989, v.A491, p.24.
142. **Bohle D., Richter A., de Jager C.W., de Vries H:** — Z. Phys., 1987, v.A328, p.463.
143. **Raduta A.A., Ursu I.I., Faessler A.** — Nucl. Phys., 1988, v.A489, p.20.
144. **Arima A., Iachello F.** — Phys. Rev. Lett., 1975, v.35, p.1069; Ann. Phys., 1976, v.99, p.253; Ann. Phys., 1978, v.111, p.201; Ann. Phys., 1979, v.123, p.468.
145. **For a review see Arima A., Iachello F.** — Adv. Nucl. Phys., 1984, v.13, p.139.
146. **Arima A., Otsuka T., Iachello F., Talmi I.** — Phys. Lett., 1977, v.B66, p.205; **Otsuka T., Arima A., Iachello F., Talmi I.** — Phys. Lett., 1978, v.B76, p.139.
147. **Sambataro M., Dieperink A.E.L.** — Phys. Lett., 1981, v.B107, p.249.
148. **Sambataro M., Scholten O., Dieperink A.E.L., Piccitto G.** — Nucl. Phys., 1984, v.A423, p.333.
149. **Wolf A., Casten R.F., Warner D.D.** — Phys. Lett., 1987, v.B190, p.19.
150. **Wolf A., Scholten O., Casten R.F.** — Phys. Lett., 1993, v.B312, p.372.
151. **Lipas P.O., Koskinen M., Harter H. et al.** — Phys. Lett., 1989, v.B230, p.1; Nucl. Phys., 1990, v.A509, p.509.
152. **Lipas P.O., Harter H., Nojarov R. et al.** — J. Phys. G: Nucl. Part. Phys., 1991, v.17, 1991, p.971.
153. **Casten R.F., Brenner D.S., Haustein P.E.** — Phys. Rev. Lett., 1987, v.58, p.658.
154. **See, for instance, Walet N.R., Brussard P.I., Dieperink A.E.L.** — Phys. Lett., 1985, v.B63, p.1.
155. **Balantekin A.B., Barrett B.R.** — Phys. Rev., 1985, v.C32, p.288; 1986, v.C33, p.1842.
156. **Bijker R.** — Phys. Rev., 1985, v.C32, p.1442.
157. **Pittel S., Dukelsky J.** — Phys. Rev., 1985, v.C32, p.335.
158. **Lo Iudice N., Palumbo F., Richter A., Wörtche H.** — Phys. Rev., 1990, v.C42, p.241.
159. **Scholten O., Heyde K., Van Isacker P.** — Phys. Rev. Lett., 1985, v.55, p.1866.
160. **Heyde K., Sau J.** — Phys. Rev., 1984, v.C30, p.1355.
161. **Oda T., Hino M., Muto K.** — Phys. Lett., 1987, v.B190, p.14.
162. **Hino M., Muto K., Oda T.** — J. Phys. G: Nucl. Phys., 1987, v.13, p.1119.
163. **Elliott J.P.** — Proc. Roy. Soc., 1958, v.A245, pp.128, 562.
164. **Arima A., Harvey M., Shimizu K.** — Phys. Lett., 1969, v.B30, p.517.
165. **Hecht K.T., Adler A.** — Nucl. Phys., 1969, v.A137, p.129.
166. **Braunschweig D., Hecht K.T.** — Phys. Lett., 1978, v.B77, p.33.
167. **Draayer J.P., Weeks K.K.J.** — Phys. Rev. Lett., 1983, v.16, p.1422.
168. **Draayer J.P., Weeks K.J.** — Ann. Phys., 1984, v.156, p.41.

169. **Rowe D.J.** — Nuclear Collective Motion, Methuen and Co.Ltd., London, 1970.
170. **Soloviev V.G.** — Theory of Complex Nuclei, Pergamon Press, Oxford, 1976.
171. **Lo Iudice N.** — Phys. Rev., 1988, v.C38, p.2895.
172. **De Coster C., Heyde K.** — Phys. Rev. Lett., 1989, v.63, p.2797.
173. **De Coster C., Heyde K.** — Nucl. Phys., 1991, v.A524, p.441.
174. **Shimano T., Ikeda A.** — Prog. Theor. Phys., 1992, v.88, p.599.
175. **Ikeda A., Shimano T.** — Nucl. Phys., 1993, v.A557, p.573c.
176. **Heyde K., De Coster C.** — Phys. Lett., 1993, v.B305, p.322.
177. **Lo Iudice N., Richter A.** — Phys. Lett., 1989, v.B228, p.291.
178. **Baznat M.I., Pyatov N.I.** — Sov. J. Nucl. Phys., 1975, v.21, p.365.
179. **Lo Iudice N.** — Nucl. Phys., 1996, v.A605, p.61.
180. **Kishimoto T., Moss J.M., Youngblood D.H. et al.** — Phys. Rev. Lett., 1975, v.35, p.552.
181. **Sakamoto H., Kishimoto T.** — Nucl. Phys., 1989, v.A501, p.205.
182. **Åberg S.** — Phys. Lett., 1985, v.B157, p.9.
183. **Åberg S.** — Nucl. Phys., 1987, v.A473, p.1.
184. **Fayache M.S., Shelly Sharma S., Zamick L.** — Phys. Lett., 1995, v.B357, p.1.
185. **Lo Iudice N.** — In: New Perspectives in Nuclear Structure, ed. A.Covello, World Scientific, Singapore, 1996.
186. **Faessler Amand.** — In: New Perspectives in Nuclear Structure, ed. A.Covello, World Scientific, Singapore, 1996.
187. **De Coster C., Heyde K.** — Phys. Rev. Lett., 1991, v.66, p.2456.
188. **De Coster C., Heyde K., Richter A.** — Nucl. Phys., 1992, v.A542, p.375.
189. **Soloviev V.G., Sushkov A.V., Shirikova N.Yu.** — J. Nucl. Phys., 1991, v.53, p.65; Iad. Fyz., 1991, v.54, p.1232.
190. **Soloviev V.G., Sushkov A.V.** — Phys. Lett., 1991, v.B262, p.189.
191. **Soloviev V.G., Shirikova N.Yu.** — Nucl. Phys., 1992, v.A542, p.410.
192. **Soloviev V.G., Sushkov A.V., Shirikova N.Yu.** — Phys. Part. Nucl., 1994, v.25, p.157.
193. **Soloviev V.G., Sushkov A.V.** — Physics of Atomic Nuclei, 1994, v.57, p.1304.
194. **Soloviev V.G., Sushkov A.V., Shirikova N.Yu.** — Nucl. Phys., 1994, v.A568, p.244; Int. J. Mod. Phys., 1994, v.E3, p.1227.
195. **Soloviev V.G., Sushkov A.V., Shirikova N.Yu.** — Phys. Rev., 1995, v.C51, p.551; Yad. Fiz., 1996, v.59, p.57.
196. **Berzins J., Prokofjevs P., Georgii R. et al.** — Nucl. Phys., 1995, v.A584, p.413.
197. **Gareev F.A., Ivanova S.P., Soloviev V.G., Fedotov S.I.** — Sov. J. Part. Nucl., 1973, v.4, p.357.
198. **Soloviev V.G.** — Z. Phys. A — Atomic Nuclei, 1989, v.334, p.143.
199. **Gallagher G.J., Moszkowski S.A.** — Phys. Rev., 1958, v.111, p.1282.
200. **Lipparini E., Richter A.** — Phys. Lett., 1984, v.B144, p.13.
201. **Soloviev V.G.** — Phys. Lett., 1965, v.16, p.308.
202. **Soloviev V.G., Nesterenko V.O., Bastrukov S.I.** — Z. Phys., 1983, v.A309, p.353.
203. **Soloviev V.G., Sushkov A.V., Shirikova N.Yu.** — J. Phys., 1995, v.G21, p.1217.
204. **Soloviev V.G.** — Yad. Fiz., 1984, v.40, p.1163.
205. **See for instance Hamamoto I.** — Nucl. Phys., 1973, v.A205, p.225; 1993, v.A557, p.515c.